2022

CALORIMETRIC MEASUREMENTS OF LUNAR REGOLITH SIMULANT AND WATER. AN EXPERIMENTAL STUDY CORRELATING WEIGHT PERCENT WATER AND TEMPERATURE CHANGE THROUGH PERIODS OF PHASE CHANGE.

George B. Johnson
Michigan Technological University, georgejo@mtu.edu

CALORIMETRIC MEASUREMENTS OF LUNAR REGOLITH SIMULANT AND WATER.

AN EXPERIMENTAL STUDY CORRELATING WEIGHT PERCENT WATER AND TEMPERATURE CHANGE THROUGH PERIODS OF PHASE CHANGE.

By

George B. Johnson

A REPORT

Submitted in partial fulfillment of the requirements for the degree of

MASTER OF SCIENCE

In Mechanical Engineering

MICHIGAN TECHNOLOGICAL UNIVERSITY

2022

This report has been approved in partial fulfillment of the requirements for the Degree of MASTER OF SCIENCE in Mechanical Engineering.

Department of Mechanical Engineering-Engineering Mechanics

Report Advisor:	*Dr. Paul van Susante*
Committee Member:	*Dr. Jeffrey Allen*
Committee Member:	*Dr. Timothy Eisele*
Department Chair:	*Dr. Jason R. Blough*

Table of Contents

1 Acknowledgments

I would like to express my deepest gratitude to Michigan Technological University's Mechanical Engineering and Engineering Mechanics department chair Dr. Jason Blough for all his hard work and assistance throughout the graduate program and for my advisor Dr. Paul van Susante who has been a big inspiration and has provided so many opportunities for myself and others in the field of aerospace. I'm extremely grateful for my committee members Dr. Jeffrey Allen and Dr. Timothy Eisele who've been so helpful and instrumental in my graduate research success. This research project endeavor would not have been possible without NASA's LuSTR 2020 research grant funding 80NSSC21K0769, because of this, my research project will likely provide utility to a whole community of lunar surface researchers.

I am also grateful for Michigan Technological University and the professors who gave me valuable instruction through my undergraduate and graduate studies. I want to give a special thanks to the Planetary Surface Technology Development Lab and all of my colleagues I had the privilege of working with, specifically Travis Wavrunek, Anurag Rajan, Benjamin Wiegand, Brian Johnson, Ellie Zimmerman, Collin Miller, and Weston Early for all of their efforts on the LuSTR 2020 thermal cone project and assistance with this research project.

I am also very thankful to my father, mother, and family for their continued support through my academic career, pushing me to complete my goals and persevere.

2 List of Abbreviations

PSRs – Permanently Shaded Regions

NASA – National Aeronautics and Space Administration

LCROSS – Lunar Crater Observation Satellite

LRO – Lunar Reconnaissance Orbiter

PSTDL – Planetary Surface Technology Development Lab

MTU – Michigan Technological University

PHCP – Percussive Hot Cone Penetrometer

LuSTR – Lunar Surface Technology Research

ISRU – In-situ Resource Utilization

Wt.% - Weight Percent

MTU-LHT-1A – Michigan Technological University, Lunar Highland Terrain 1A

3 Abstract

Permanently Shaded Regions (PSRs) are cold traps located around the lunar south pole that have been confirmed to contain possible interesting quantities or volatiles such as H_2O, CO_2, SO_2, CH_4, and others. [1] The identification of these volatiles on the lunar surface was a critical step in the development of NASA's strategic goals for scientific discoveries, sustained space travel and exploration, and re-establishing a human presence on the moon. These volatiles are vital to the future of operating in and exploring space. The LCROSS impact revealed the existence of these resources in PSRs but more information is needed about the volatile quantities and distributions present in these cold traps before resource extraction missions can be designed. Determining the location and distribution of these resources can be accomplished through ground truthing and actively sampling the lunar surface. Currently, the primary methods of sampling or prospecting the lunar surface are drilling and core sampling.

The Planetary Surface Technology Development Lab (PSTDL) at Michigan Technological University (MTU) has secured funding through NASA's Lunar Surface Technology Research (LuSTR) 2020 initiative for proposing an alternative prospecting instrument called the Percussive Hot Cone Penetrometer (PHCP). Dynamic cone penetrometers are used in terrestrial applications to provide geotechnical information about soils. The PHCP seeks to combine a modified design of a dynamic cone penetrometer and thermal calorimetric measurements to identify strategic volatiles buried in the lunar regolith. Testing and development of the thermal measurement system for the PHCP are discussed in this report. Experimental testing was conducted to validate the methods by which volatile concentrations will be identified. These test results were utilized in the design of the PHCP and in the validation of a thermal model to predict weight percentages of volatiles based on observable temperature data. Detecting regions of volatile phase change allows for the concentration of the identifiable volatile to be estimated to be within ± 1 wt.%. The data collected and outlined in this report was used to determine a method for estimating the weight percentage of a mixed sample, and was successful in approximating the weight percentage of the test data, but requires further consideration to apply it successfully across more weight percentage mixtures and power levels.

This report will cover the development of multiple experimental test campaigns, their respective results, and design implications, as well as the continued development of a thermal cone instrument for integrated PHCP testing and validation.

4 Prospecting the Lunar Surface

It is important to understand the goals and motivations behind researching a method for mapping lunar volatile concentrations and distributions in lunar cold traps.

4.1 Background

NASA has a series of ARTEMIS missions that are committed to returning humans to the moon to establish a more permanent presence there. The main reason behind establishing a presence on the lunar surface is the resources contained in the regolith. These resources include water, carbon dioxide, methane, metals, and more.

NASA has identified key resources that are likely to be found in certain places on the lunar surface. Information obtained using neutron and IR spectroscopy on the plume created by the LCROSS impact into the Cabeus crater confirms the presence of water ice in permanently shaded regions (PSRs). [1] These findings are important because water, and other volatiles, collected in space save time and money, reduce risks of sending resources to space, allow for the possibility of sustained human presence on the moon, and provide rocket fuel for further space exploration. However, the results obtained from the LCROSS impact only provide a preliminary glance at the resources present and not the quantity or distribution of volatiles in a PSR. Knowing the concentration of volatiles in a PSR is presently the immediate need of the lunar space industry. Before sending excavation and extraction equipment to the moon, the location and distribution of the resources intended to be collected need to be known.

As a part of this initiative to support ARTEMIS, NASA uses the Lunar Surface Technology Research (LuSTR) grant funding to accept technology proposals for key areas of space research. Within this program, Michigan Technological University's Planetary Surface Technology Lab (PSTDL) proposed a design for an In-situ Resource Utilization (ISRU) prospecting device that would not only help identify volatiles and their concentrations in a PSR but provide geotechnical data about the regolith found there too.

4.1.1 Accessibility Notes

To read more about NASA's goals for the moon, mars, and beyond please visit: https://www.nasa.gov/specials/artemis/

4.2 Introduction

The research conducted, as outlined in this report, relates to the design of a Percussive Hot Cone Penetrometer (PHCP). This PHCP was the proposed technology the PSTDL submitted to NASA's LuSTR 2020 grant as an ISRU prospecting instrument. In practice, the PHCP will provide geotechnical measurements of lunar regolith in a Permanently Shaded Region (PSR) as well as detect the presence and quantity of volatiles.

The PHCP is designed to stop at 10 cm increments along a 1-meter-deep percussive test. At each 10 cm increment, an embedded heater will apply heat to the surrounding regolith. Through the measurement of temperatures at points along the exterior of the cone instrument, regions of volatile phase change will be measured. Once a phase change region has been observed, the temperature and pressure at the time of its occurrence will be enough to identify the volatile species. Further, the research presented in this report shows experimental data of tests conducted in regolith simulant at various temperatures under atmospheric pressure to validate this method of volatile detection. This set of data will help inform a computer model of water phase change in regolith simulants under extreme conditions. Additionally, these tests informed the design of the PHCP and the thermal cone testing procedure.

5 Calorimetric Experiments

5.1 Experimental Methods

5.1.1 Experiment Concept

The PHCP's method of detecting lunar volatiles and quantifying their abundance by adding heat energy and measuring the temperature profiles of the surrounding sample material needed to be validated. Specifically, the achievable accuracy, or the ability to detect the weight percentage of a volatile to within ± 1 wt.%. This accuracy requirement was established in the project proposal required by NASA and guided this research. If an identifiable volatile such as H_2O exists in the lunar regolith, then the weight percentage of the volatile can be determined to an accuracy of at least ± 1 wt.%.

It is important to validate this hypothesis with experimental data to inform the design of the PHCP and assure the proposed method of volatile detection and quantification will work. The results from experimental testing will be used to validate a computational thermal model of the PHCP that will achieve this desired accuracy.

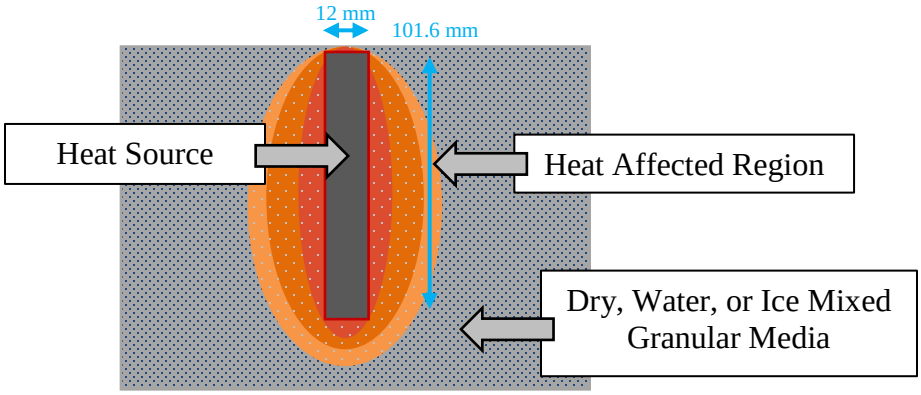

Figure 1: Initial experimental design concept showing a submerged heat source and the expected behavior of heat conduction (temperatures in the granular media relative to the heat source)

The first series of experimental tests were conducted at standard atmospheric pressure and were intended to determine the size of the heat-affected region within silica sand samples mixed with 0, 5, and 10-weight percentages of water or ice inclusions (Figure 1). This was accomplished by measuring temperatures within a mixed sample at increased distances from the heat source. F-80 silica sand was initially used as a reference granular media because the thermal and mechanical properties were known and due to the limited availability of our newly produced lunar simulant MTU-LHT-1A at the start of testing. The weight percentages of water and water ice were initially chosen to be 0, 5, and 10 because a dry sample, 0 wt.% water, serves as a baseline for extracting the heat capacity, thermal conductivity, and diffusivity of the granular media, 5 wt.% water is close to some estimates of water ice concentrations in lunar cold traps, and 10 wt.% water is closer to fully saturating the silica sand material which provides a useful edge case. [1]

Table 1 shows an outline of the experimental tests that were conducted at three distinct constant power levels all at standard atmospheric pressure. These constant power levels of 30, 50, and 100 Watts were determined by preliminary tests conducted in dry, 5wt% wet, and 10wt% wet mixed silica sand samples. Samples with a greater weight percentage of water required more power to detect regions of phase change because of increased thermal diffusivity due to the water content. The effects of this resulted in a larger heat-affected region as will be discussed further in the results section 2.3. Table 1 also shows the second and third series of experimental tests that were designed to measure the heat-affected region in mixed lunar regolith simulant MTU-LHT-1A samples with weight percentages of water between 0 and 5 wt.% and between 5 and 10 wt.% because detecting intermediate weight percentages of water or water ice aided in the accuracy verification of the measurement technique.

Table 1: Number of experimental tests conducted at ambient pressure and constant power levels for various sample materials mixed with specific weight percentages of water or ice

Sample Material and Volatile Composition	**Constant Power Supplied**		
	30 Watts	**50 Watts**	**100 Watts**
Dry, F-80	3	3	2
Wet 5 wt.%, F-80	1	1	1
Wet 10 wt.%, F-80	-	1	1
Frozen 5 wt.%, F-80	-	1	1
Frozen 10 wt.%, F-80	-	1	1
Dry, MTU-LHT-1A	1	1	1
Wet 1.5 wt.%, MTU-LHT-1A	1	1	1
Frozen 1.5 wt.%, MTU-LHT-1A	1	1	1
Wet 5 wt.%, MTU-LHT-1A	1	1	1
Frozen 5 wt.%, MTU-LHT-1A	1	1	1
Wet 7 wt.%, MTU-LHT-1A	1	1	1
Frozen 7 wt.%, MTU-LHT-1A	1	1	1
Wet 10 wt.%, MTU-LHT-1A	-	1	1
Frozen 10 wt.%, MTU-LHT-1A	-	1	1

5.1.2 Experiment Design

A simple test setup utilizing a buried cartridge heater and thermocouples was designed to measure temperatures within the various mixed granular media samples. Specifically, a ½" diameter, 4" long high density 120 V AC cartridge heater (Omega: HDC00545) with a maximum wattage, watt density, and maximum temperature of 750 W, 21 W/cm^2, & 760^{o}C respectively was sourced and available in our lab inventory. Controlling and measuring the constant power supplied to this heater provided a constant heat source for the duration of each test. Temperature measurements were to be recorded using up to a total of (24), 24 AWG K-type thermocouples implanted in the granular media mixed sample at 5 mm incremental distances from the surface of the cartridge heater up to a total distance of 40 mm (Figure 2). Considering the maximum heat-affected region to be measured was 40 mm from the surface of the cartridge heater, a modified 5-gallon bucket was large enough to use as a test container without edge effect concerns on the outer thermocouple measurements. Figures 2 & 3 show the layout of the thermocouples embedded in the mixed granular media sample and the test setup layout with the modified bucket, cartridge heater, and thermocouple positions.

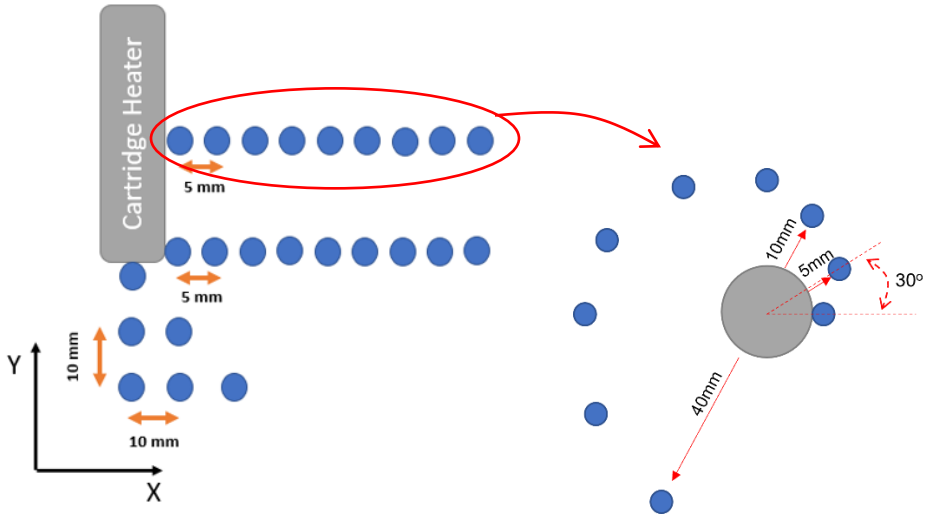

Figure 2: Simplified cross-sectional views of the 24 type-K thermocouples (blue circles) 5 mm incremental positions relative to the cartridge heater

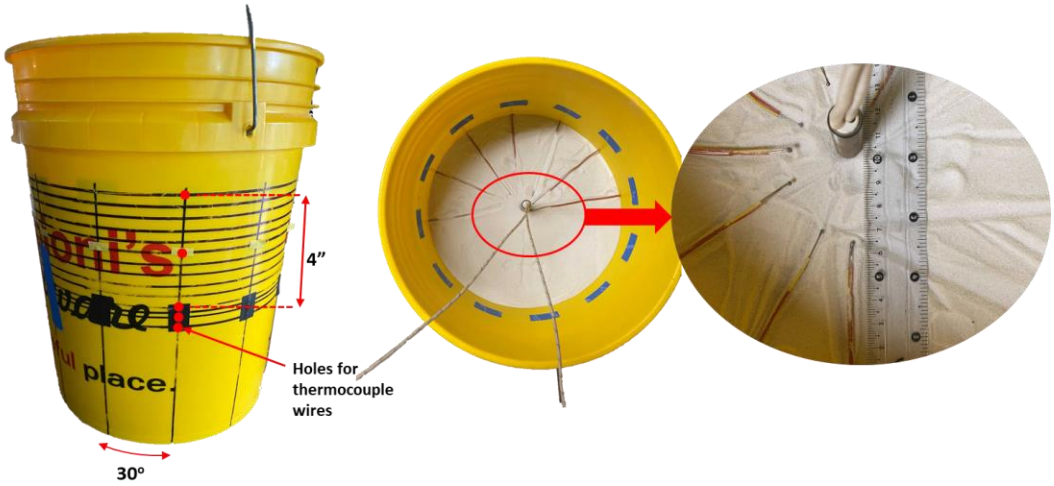

Figure 3: Experimental test setup utilizing a modified 5-gallon bucket with holes for type-K thermocouples that are positioned at 5 mm increments from the surface of the cartridge heater.

Temperature data for these tests were recorded using a national instruments compact data acquisition chassis (cDAQ) and analog voltage input modules NI-9213 and NI-9211 for measuring thermocouples. Power to the cartridge heater was controlled using a variable AC (VARIAC) unit and was measured using an Arduino microcontroller paired with a Dr. Wattson 15A capacity power logger (Figures 4 & 6). Information from the Arduino serial output was read by a NI LABVIEW program and output to the user interface along with the temperature data from all 24 thermocouples (Figure 5). All time-dependent temperature and power data were then saved to a single .csv file. This data acquisition hardware and method was chosen because of the familiarity with microcontrollers and LABVIEW software as well as the ability of the NI modules to read more accurately, filter, digitize, and save a greater number of thermocouples inputs.

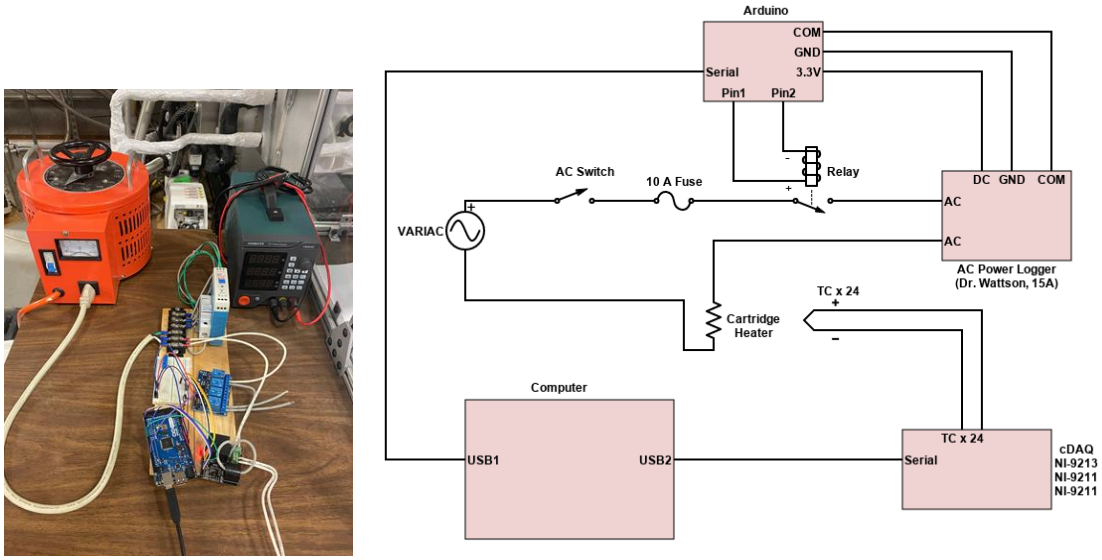

Figure 4: VARIAC power supply, power logger, NI cDAQ with thermocouple analog voltage modules, and DAQ schematic

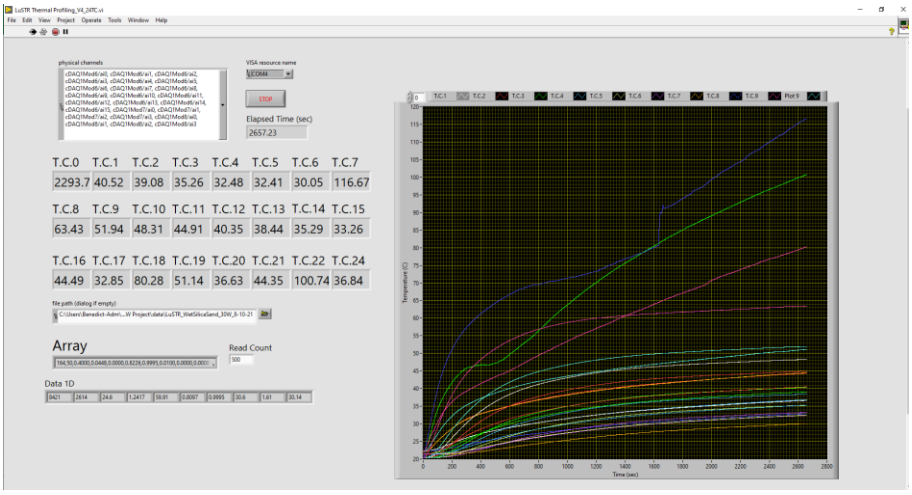

Figure 5: LABVIEW user interface panel displaying 24 real-time temperature measurements along with voltage, current, and power data.

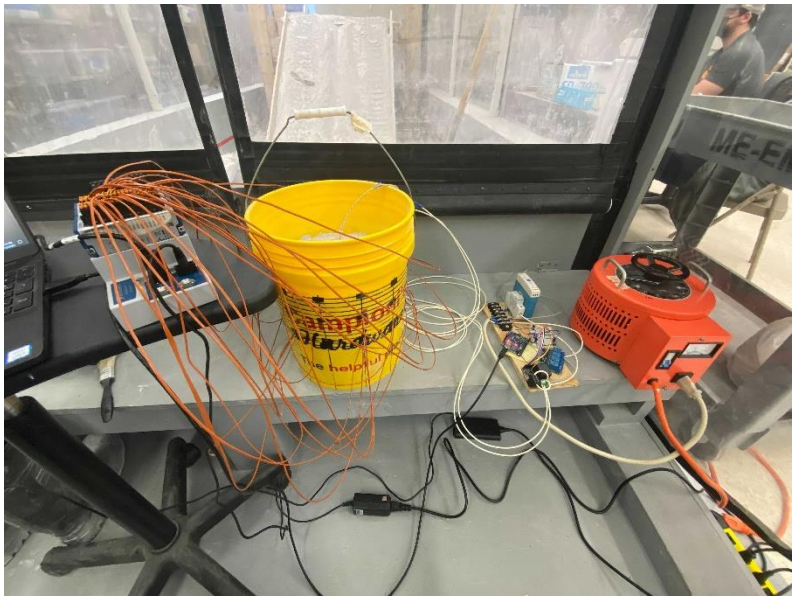

Figure 6: Complete LuSTR20 thermal cartridge heater test setup with power supply, power logger, cDAQ, and thermocouples mounted in a mixed sample being tested at ambient conditions

5.1.3 Reference Material and Hardware Evaluation

The choice to use F-80 silica sand as a reference granular media was made because the mechanical and thermal properties of the material were better known than our newly produced MTU-LHT-1A lunar simulant. However, this sand was used from an existing stockpile, and information on the particle size distribution was no longer available from the original supplier. Understanding the particle size distribution of this reference granular material was necessary for approximating mechanical and thermal characteristics as well as correlating these characteristics with the primary test material MTU-LHT-1A. A sieve analysis was conducted on the F-80 silica sand material and the results are shown in Table 2 and Figure 7 below.

Table 2: F-80 Silica Sand Particle Size Distribution, Percent Passing

F-80 Silica Sand – Sieve Test Results		
>300 µm	22.0 g	2.81 %
300 > x >212 µm	237.0 g	30.26 %
212> x >147 µm	270.3 g	34.52 %
147 > x >104 µm	214.2 g	27.35 %
104 > x >74 µm	34.9 g	4.46 %
74 > x >53 µm	3.9 g	0.50 %
<53 µm	0.8 g	0.10 %
	783.1 g	100 %

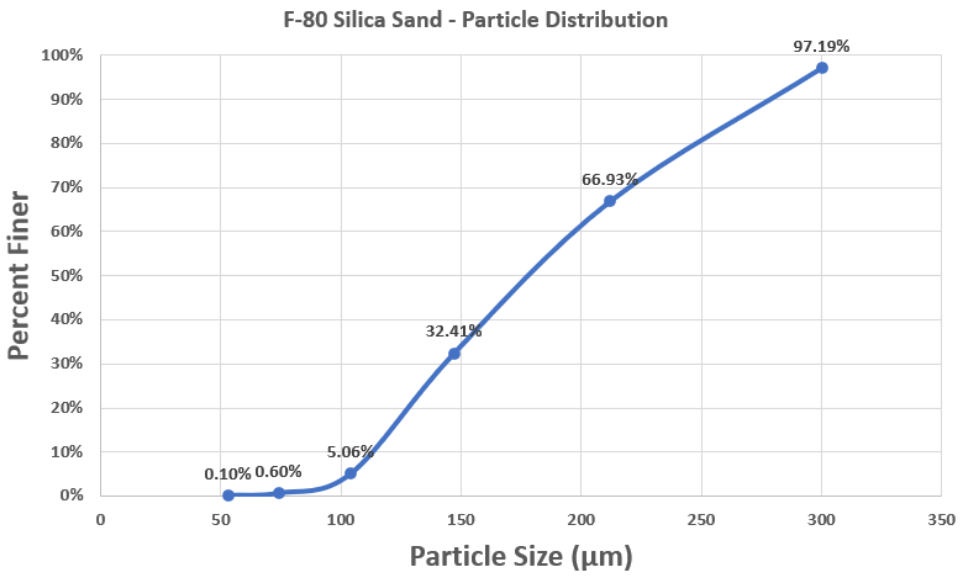

Figure 7: Graphical representation of sieve analysis results for the reference material F-80 silica sand particle size distribution, cumulative percentage of particles.

The performance of the high-density cartridge heater was also unknown at the start of these experimental tests. Figure 8 shows images from a thermal camera taken 20 seconds apart as a constant 30 Watts was applied to the fully exposed cartridge heater. The temperature gradient along the exterior of the heater was larger than expected as the top one inch of the heater was consistently much cooler than the mid-section and bottom end. This was useful in determining the placement of the thermocouples surrounding the heater and is the reason why the midsection, endpoint, and underside of the heater were chosen as target areas for temperature measurement.

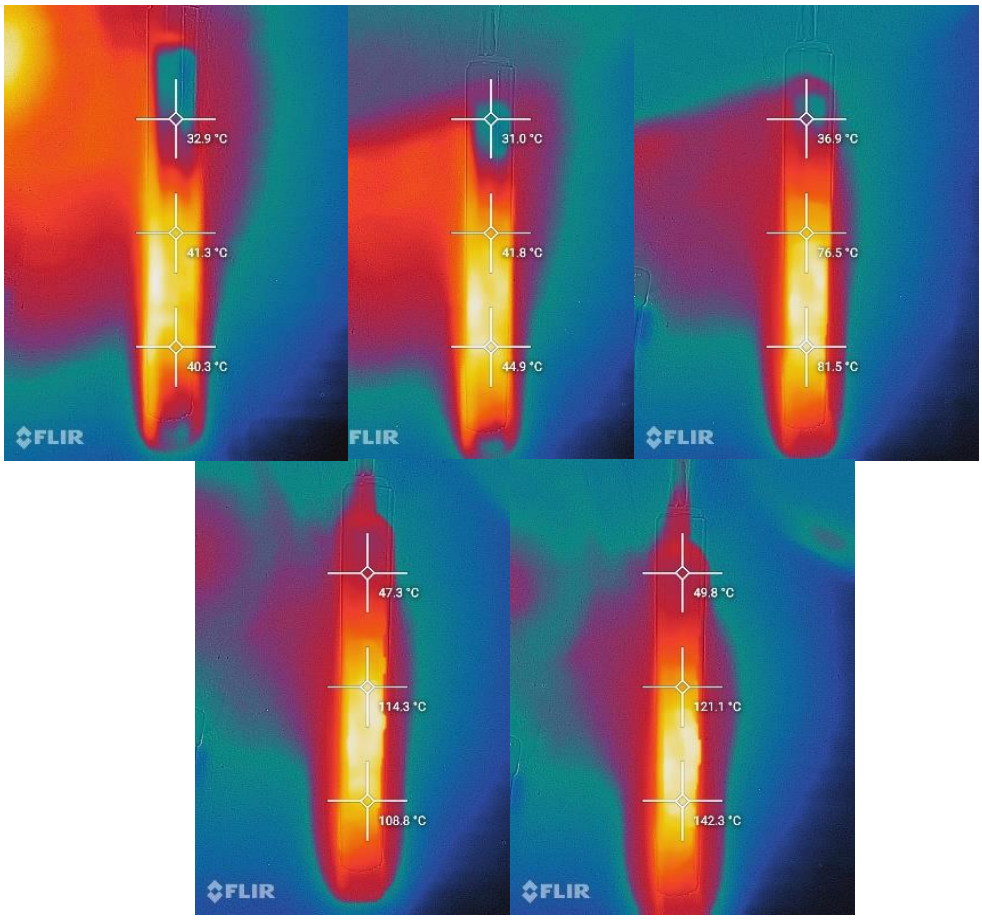

Figure 8: 20-second interval thermal images of the completely exposed cartridge heater as a constant 30 Watts was applied

5.2 Experimental Procedure

5.2.1 Mixed Sample Preparation

To effectively test the heat propagation through different mixed F-80 silica sand or MTU-LHT-1A samples water or discrete ice shavings need to be evenly distributed within the sample. Procedures for mixing the initial F-80 silica sand samples are the same as mixing the lunar simulant and therefore references in this procedure to the lunar simulant preparation procedure apply to the silica sand samples as well.

The primary method of ensuring the content of water or ice was to mix water with the lunar simulant and freeze the sample after the test setup procedure. This produced a concreted frozen sample which was easiest to reproduce. Another method to control the weight percentage of ice was to use discrete ice shavings. This method was also considered for testing as there are many proposed methods of lunar ice deposition and discrete ice particles

are likely more representative of the deposition phenomena on the moon than concreted frozen samples. [2] However, the sample preparation method of mixing discrete ice particles requires the sample to be produced in a chilled environment. Time constraints limited the number of tests conducted and no tests were conducted using this preparation procedure, however, plans for future testing with the thermal cone will include this method as the method of ice deposition in the granular media is a variable of interest.

An even mixture of water and lunar simulant was achieved using a polyethylene-walled concrete mixer and hand pump sprayer (Figure 9). Water was atomized and slowly added to a desiccated pre-weighed sample of MTU-LHT-1A via a hand pump sprayer. The specific quantities of water as a weight percentage of the regolith sample were achieved by weighing the dry regolith simulant and measuring either 1.5 wt.%, 5 wt.%, 7 wt.%, or 10 wt.% of water as it was added to the hand pump sprayer on a digital scale.

Figure 9: Procedure for mixing a sample with an even distribution of a specific weight percentage of water.

After the water was added to the MTU-LHT-1A sample, the mixed sample was collected and weighed again in a 5-gallon bucket to validate the water content added. In addition to this, small quantities of the mixed sample were collected, weighed, desiccated in a 100^{o}C oven, and re-weighed. Typically, two to three of these smaller samples were fully desiccated and weighed in this manner to provide an average measurement of the water content used in each test.

Figures 10 & 11: (1) Weighing the dry sample of regolith to determine wt.% of water. (2) Post-mixture weighing small desiccated mixed samples for water content validation.

5.2.2 Test Setup Procedure

Once the dry or mixed sample of F-80 silica sand or MTU-LHT-1A lunar simulant was prepared, the test bed was set up using the procedure listed below.

1.) Add small quantities of mixed or dry samples to the testing container and uniformly compact them into 2-to-3-inch layers until the compacted layer reaches the bottom thermocouple layer (Figures 12 - 15).

2.) Insert the first 3 K-type thermocouples through the exterior of the 5-gallon bucket in pre-drilled hole locations 30^{o} apart. Center the first welded thermocouple bead in the bucket and measure 10 mm and 20 mm spacings from the center point for the remaining two thermocouples. Thermocouple placement error should not exceed ± 1 mm. (Figures 16 & 17)

3.) Gently add a small amount of dry or mixed material on top of the first layer of thermocouples to make up a 10 mm thick compacted layer. Ensure the thermocouples don't move by holding each wire as the material is added and uniformly compacted.

4.) Complete the pattern of thermocouple placement under the heater as seen in Figure 2 by adding 10 mm layers of compacted material on each layer of thermocouples until the layer height reaches the cartridge heater's desired location.

5.) Add the 6th underside thermocouple centered in the bucket and place the cartridge heater directly on top of it so that the thermocouple is in contact with

the bottom of the heater. The heater was maintained vertically by suspending it via the lead wires tied to the bucket handle. (Figure 17)

6.) After adding the cartridge heater, insert the next 9 thermocouples at 30^{o} intervals around the exterior of the bucket and position the thermocouples at 5 mm increments from the exterior sheath of the heater. The first thermocouple will start directly in contact with the heater sheath. (Figure 18)

7.) Once all 9 thermocouples are added to this layer, gently add a small amount of dry or mixed sample material and evenly compact it until the midpoint of the heater is reached.

8.) Repeat step 6 at a layer height 2 inches above the last thermocouple layer, or the midpoint of the cartridge heater.

9.) Repeat step 7 until the dry or mixed sample material reaches the top of the cartridge heater. (Figure 19)

10.) Stop here if the test is for a dry or wet test, otherwise cover the top of the bucket and place it in a freezer to make a concreted ice sample. Of the remaining material fill two to three smaller containers and take weight measurements for moisture content verification.

11.) After completing the test setup weigh the compacted sample on a digital scale and record the mass in kg. Take measurements of the larger test setup column height and the final diameter at the top of the bucket to use for bulk density calculations.

12.) Desiccate the smaller collected samples in a 100^{o}C oven and record the mass after 24 hours or when the samples are completely dry. Calculate the mass difference between the mixed and dry samples to verify the target wt.% of water for that individual test setup.

13.) Record the environmental conditions that the sample was prepared in, such as barometric pressure, ambient temperature, and humidity. Connect the bare thermocouple leads to the NI data acquisition modules and begin the testing procedure.

Figures 12 - 15: Test setup steps number 1, adding mixed silica sand sample, uniformly compacting 2-to-3-inch layers until the first thermocouple layer is reached.

Figures 16 - 19: Test setup steps 2 through 9, inserting thermocouples and measuring their placement in mm relative to the cartridge heater placement, adding mixed silica sand sample and compacting layers to the top of the cartridge heater.

5.2.3 Testing Procedure

Once the test setup is complete and the mixed sample is ready for standard atmospheric testing before power was applied, the variable AC power supply (VARIAC) was set to the predetermined voltage of 24.7 V, 31.7 V, or 45 V to test at a constant 30 W, 50 W, or 100W respectively. These voltages were determined for the specific high-density cartridge heater used in these tests and remained consistent across all tests conducted.

After setting the VARIAC to the proper voltage, the microcontroller and power logger as well as the NI cDAQ were initialized and their respective codes were executed to verify the channels on the analog voltage input modules are reading correctly and that the temperature values being recorded were within agreeable tolerances (±2.2^{o}C for type-K thermocouples). The file path directories were set and both series of code was re-initialized on the microcontroller and cDAQ then power was immediately supplied by manually switching on the VARIAC unit.

Once the test began, the temperatures recorded by the thermocouples in contact with the cartridge heater increased immediately. Regions of phase change were observable from the LABVIEW UI graphical display as the temperatures immediately surrounding the heater passed 0 ^{o}C (for mixed ice tests) and near 100 ^{o}C. Power was continuously applied for at least an hour until regions of phase completed for the first two thermocouples in the midpoint region of the heater or until a ceiling temperature of 600^{o}C was observed. Upon either of these conditions, power was then cut by switching off the VARIAC. Temperature data continued to be collected for an additional 45-minute period as the sample began to cool down and temperatures converged.

After this period of a 45-minute cooldown, the LABVIEW code was terminated, and the data file was saved. Thermocouple connections were disconnected from the NI modules and the sample test setup was re-weighed. Considering the size of the sample, not all tests had distinguishable differences in their post-test weights. After recording this data and collecting the moisture content verification data from the smaller desiccated samples the test was effectively complete. The test setup was disassembled, and the mixed sample was put on baking trays and desiccated to ensure the sample material was ready for the next preparation process.

5.3 Results and Discussion

5.3.1 F-80 Silica Sand Samples

5.3.1.1Results & Analysis

F-80 silica sand was used as the base granular media for initial testing because the thermal and mechanical properties have been tested and are well documented. The thermal conductivity of silica sand as reported by material-properties.org is 0.25 $W/(mK)$ and the specific heat is around 750-830 $J/(kgK)$. The bulk density of silica sand is reported to be 1500 kg/m^3 which aligns closely with the measured bulk density of dry F-80 silica sand, 1550 kg/m^3, used for testing. [3,4] Bulk densities were calculated for all tests by first calculating the volume of a truncated cone, the approximation of the volume of the sample in a 5-gallon bucket, using the measured dimensions of the 5-gallon bucket test bed and the column height of the sample material in addition to the measured sample mass.

Dry silica sand samples were tested first to outline the test setup procedure and to measure baseline temperature profiles and the size of heat-affected regions for constant 30 W, 50 W, and 100 W. Temperature results from the dry 30 W silica sand tests can be seen in Figures 20 - 22 for regions surrounding the cartridge heater's midsection, endpoint, and underside. The size of the heat-affected zone radially outward from the heater's midsection was greater than the observed heat-affected region at the base or underside of the heater. These temperature profiles show that throughout an hour heat was conducted through the dry sand samples out to a distance of at least 40 mm, raising the temperature of the sand surrounding the furthest thermistor by ~23 ^{o}C. The temperature difference observed at the midpoint of the heater between the thermocouple in contact with the cartridge heater and the thermocouple 5 mm away from the cartridge heater surface was over 50 ^{o}C after a short

period of 800 seconds (Figure 20). This difference indicates the insulative properties of this granular material and likely includes a small degree of thermocouple placement error of roughly ± 1 mm.

Assuming that the thermocouple in contact with the cartridge heat is 5 mm away from the second thermocouple along the midsection of the heater, the thermal conductivity calculated using equation 1 averaged about 0.38 $W/(mK)$. Given an error estimation of ± 1 mm, the range of possible thermal conductivity is between 0.31 and 0.47 $W/(mK)$. The heat rate Q was the constant power supplied to the heater 30 W, 50 W, or 100 W. dT was calculated by taking the difference between the temperature data for the thermocouple in contact with the heater and the temperature data for the thermocouple located 5 mm away. r_o & r_i were assumed to be the radius of the cartridge heater (0.006 m) and the radius of the thermocouple 4 to 5 mm from the heater surface (0.010 to 0.011 m) respectively. The thermal diffusivity of dry silica sand can be calculated using equation 2, taking the thermal conductivity of 0.38 $W/(mK)$ and dividing it by the density, 1500 kg/m^3, times the specific heat capacity at constant pressure, 750 $J/(kgK)$, yielding a result around 3.38e-07 m^2/sec.

$$Q = 2 \cdot \pi \cdot k \cdot L \cdot \frac{(T_2 - T_1)}{\ln(\frac{r_o}{r_i})} \quad (1)\ [5]$$

$$\alpha = \frac{k}{\rho * c_p} \quad (2)$$

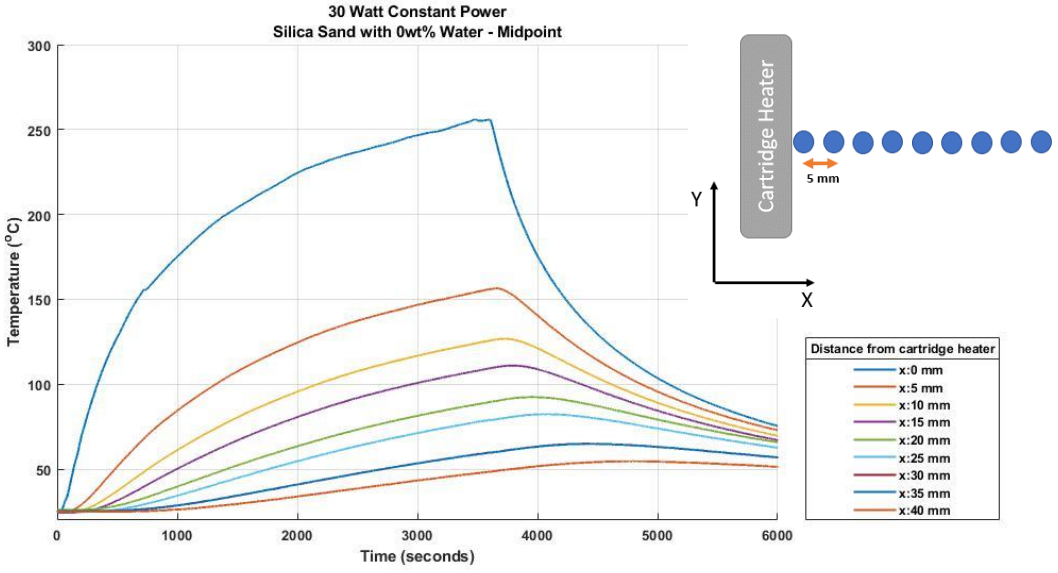

Figure 20: Temperature profiles observed for constant 30W tests in desiccated silica sand sample surrounding the midsection of the cartridge heater at 5 mm incremental distances from in contact with the heater to 40 mm in the sample.

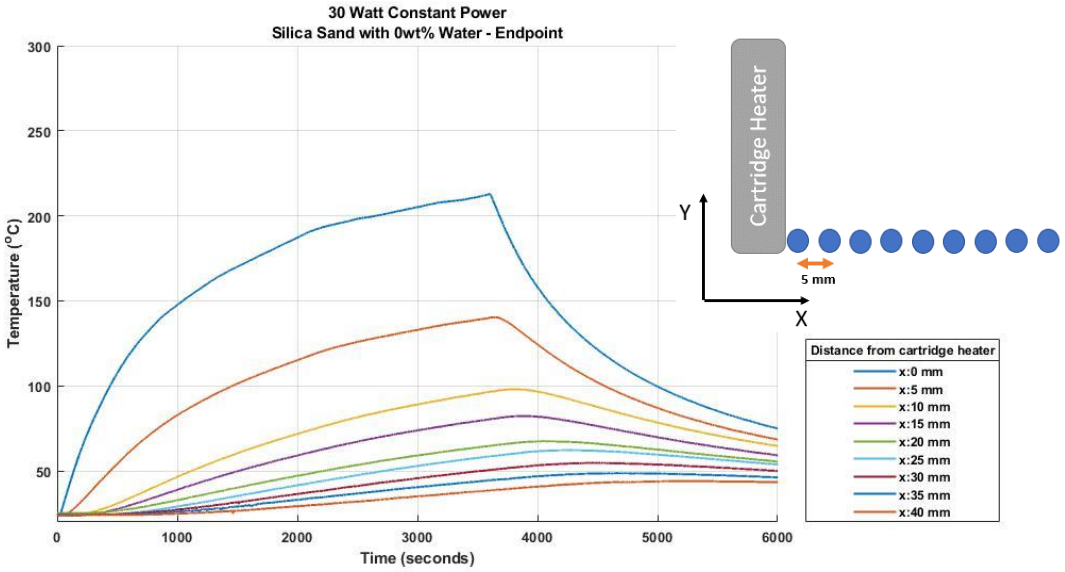

Figure 21: Temperature profiles observed for constant 30W tests in desiccated silica sand sample surrounding the bottom edge or "endpoint" of the cartridge heater at 5 mm incremental distances from in contact with the heater to 40 mm in the sample.

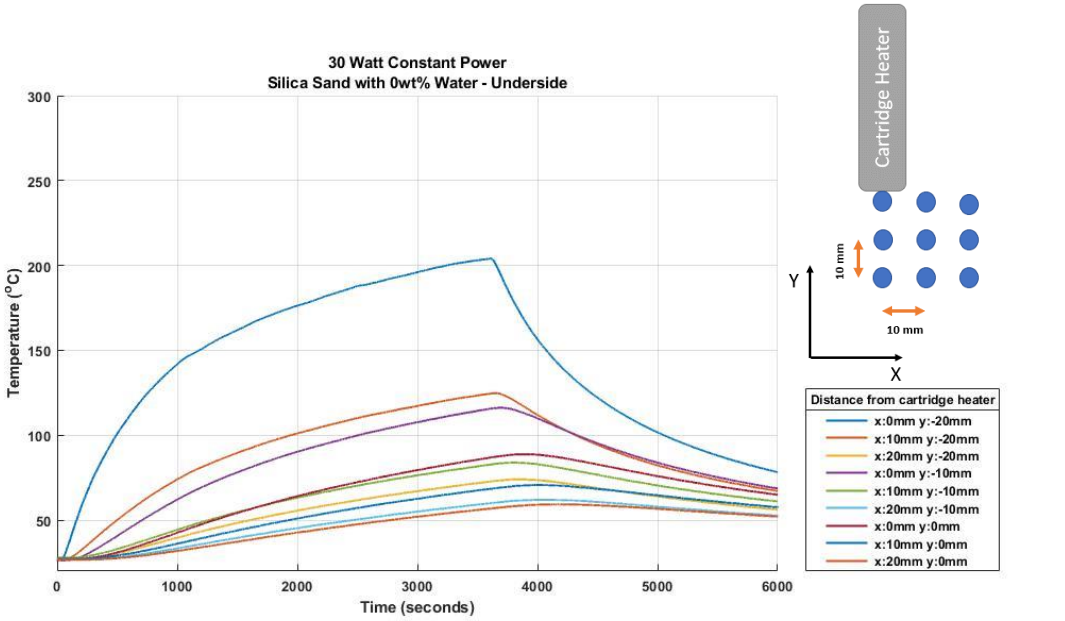

Figure 22: Temperature profiles observed for constant 30W tests in desiccated silica sand sample surrounding the underside of the cartridge heater in an array of equally spaced 10 mm distances.

The midsection of the cartridge heater is used for all further analysis of heat-affected regions and volatile weight percentage correlations as this is the region where the most consistent phase change observations occurred. After conducting tests with dry silica sand and validating the thermal properties of the base granular media, specific weight percentages of water were mixed with each sample and tested using the same method. Results from water and ice inclusions at 5 weight percent and 10 weight percent can be seen in Figures 23 - 29 as well as the effects of increased wattages on the period of observable phase change. 30 W tests were not conducted on samples containing 10 wt.% water or ice because the amount of power was insufficient to raise the temperature of the sample to effectuate phase change in a reasonable period. 50 W proved to be insufficient for 10 wt.% water samples as well (Figure 26).

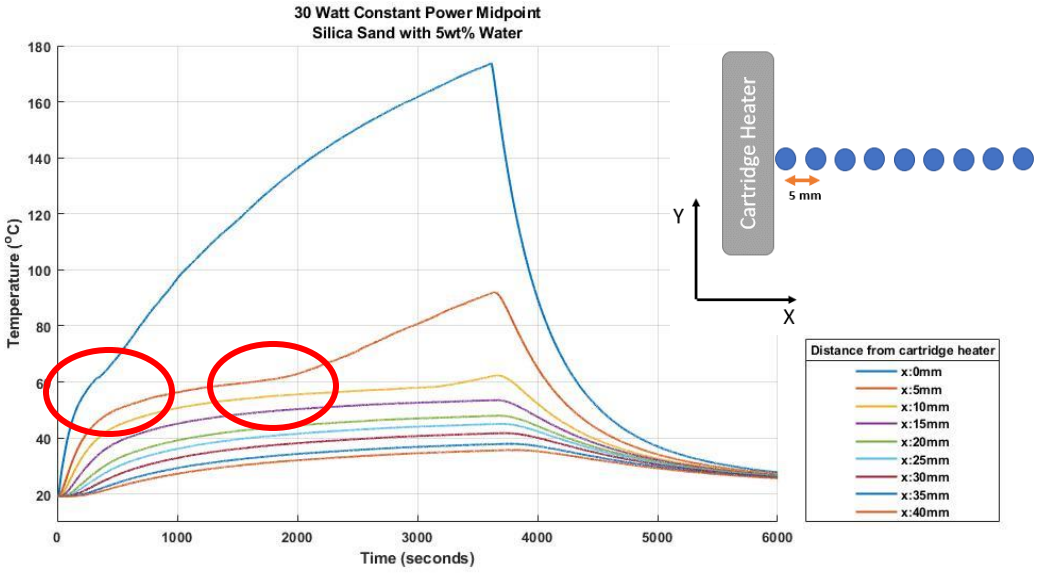

Figure 23: Temperature profiles around the cartridge heater midsection observed for constant 30W tests in silica sand samples mixed with 5 wt.% water

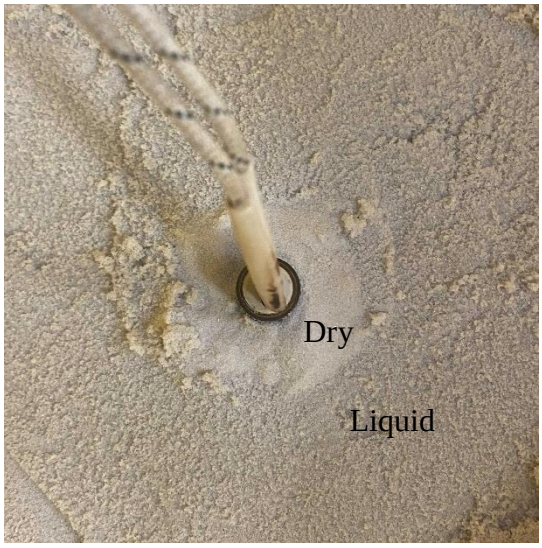

Figure 24: 30-Watt test with 5 wt.% water mixed with silica sand, post-test dry region observation

An interesting observation of the temperature profiles for 0 mm and 5 mm from the cartridge heater surface show an inflection point around 60°C for 5 wt.% water samples conducted at 30-Watt, 50-Watt, and 100-Watt. This was consistently observed across all 5 wt.% water mixed samples and could be explained by the migration of vapor through the porous granular media as the pressure inside the sample is likely increasing in conjunction with the increase in temperature. Localized pressure changes weren't measured and thus this possible explanation wasn't validated for these tests.

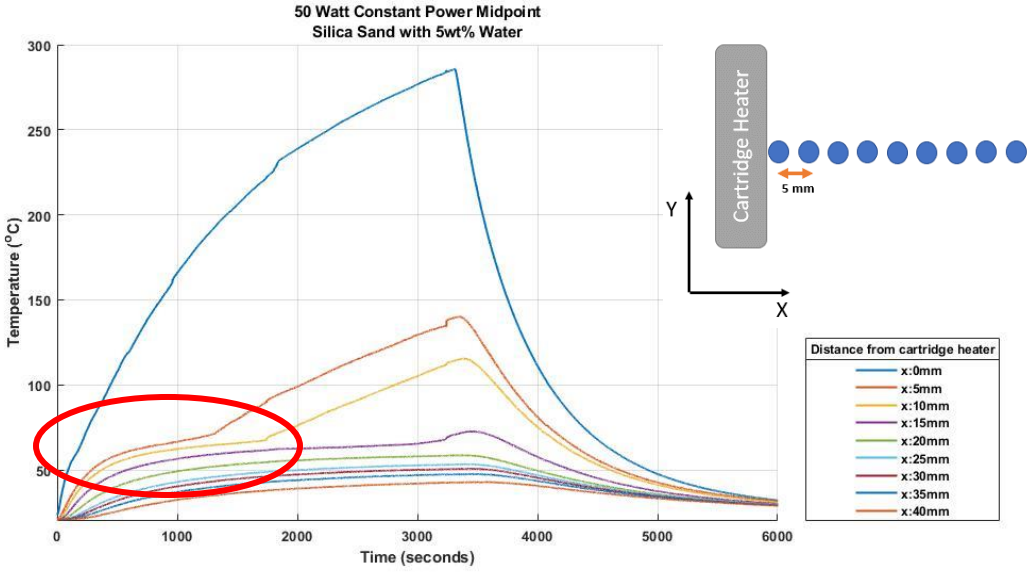

Figure 25: Temperature profiles around the cartridge heater midsection observed for constant 50W tests in silica sand samples mixed with 5 wt.% water

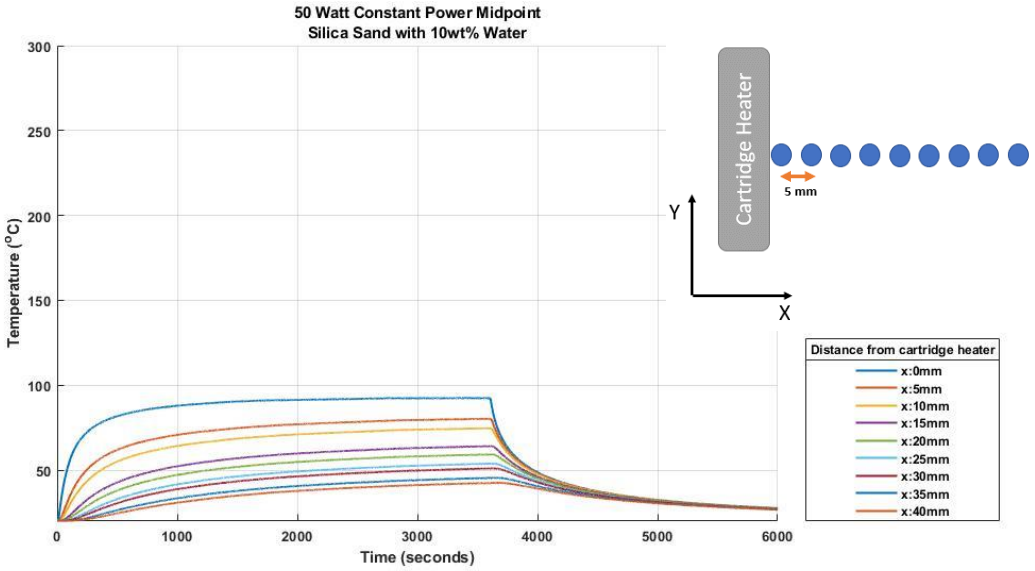

Figure 26: Temperature profiles around the cartridge heater midsection observed for constant 50W tests in silica sand samples mixed with 10 wt.% water.

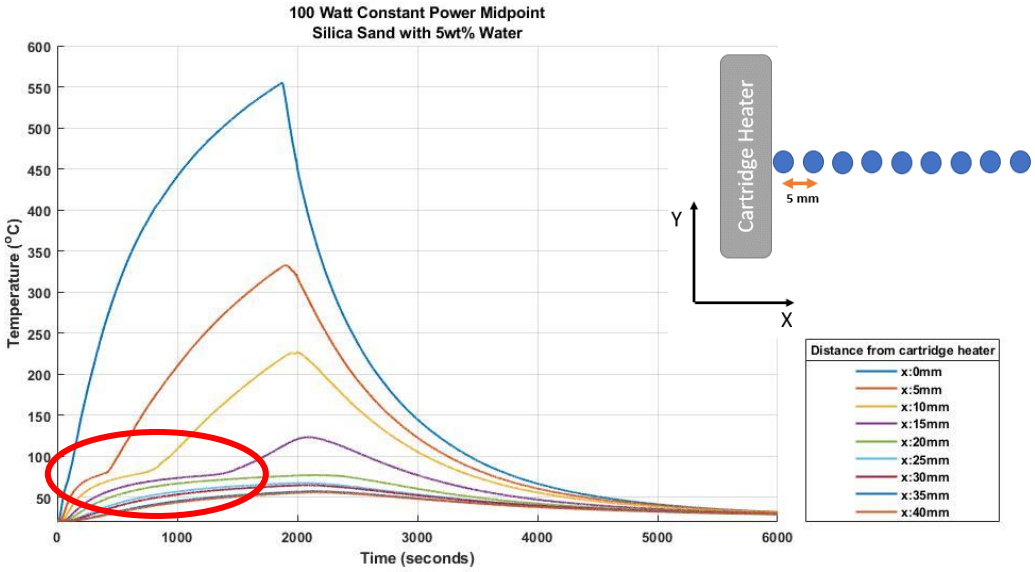

Figure 27: Temperature profiles around the cartridge heater midsection observed for constant 100W tests in silica sand samples mixed with 5 wt.% water.

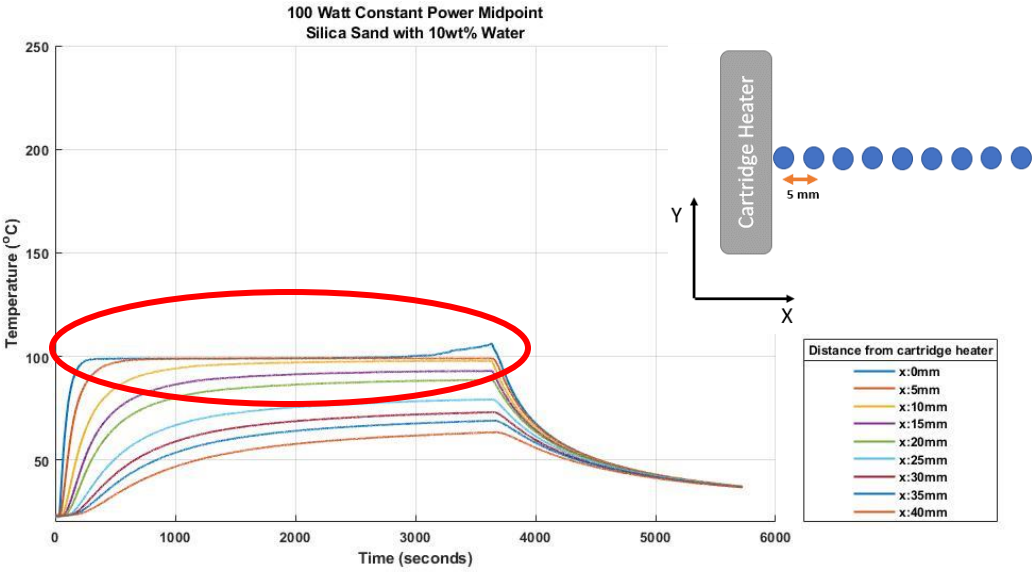

Figure 28: Temperature profiles around the cartridge heater midsection observed for constant 100W tests in silica sand mixed with 10 wt.% water.

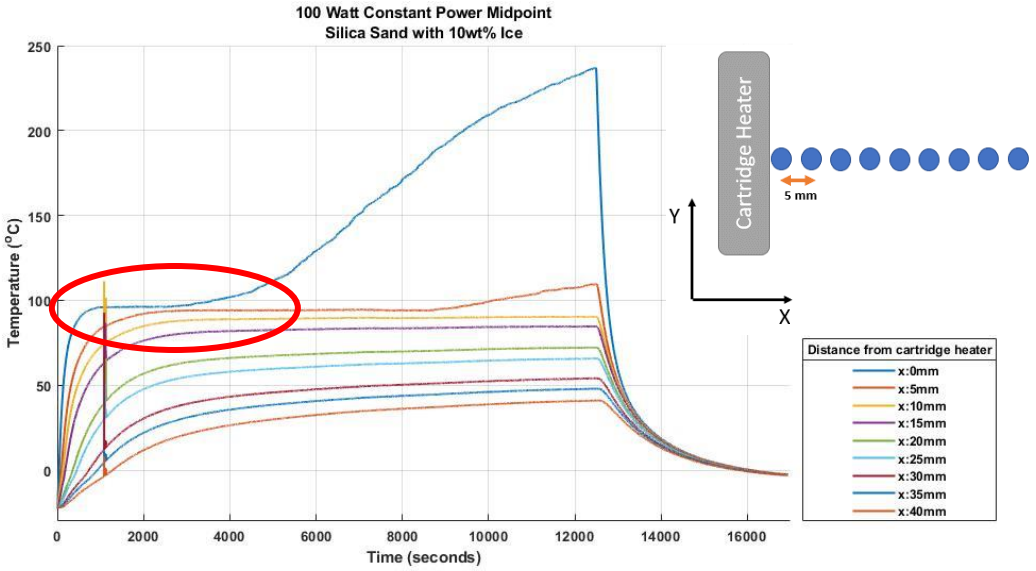

Figure 29: Temperature profiles around the cartridge heater midsection observed for constant 100W tests in silica sand with 10 wt.% cemented ice.

The period of phase change for 10 wt.% water and 5 wt.% water mixed samples is distinguishable by the region of latent heat observed in the temperature profiles. Measuring this period and correlating the time between inflection points with the weight percentage of water will provide a metric for estimating water content in mixed samples. Further analysis will be conducted on these results in addition to more testing. The results from these mixed silica sand samples in addition to the tests with MTU-LHT-1A regolith simulant will be used in the formulation of a computational model of heat transfer and phase change. Computer modeling will be used to supplement the number of experimental tests needed to draw conclusive correlations between volatile content and the observable regions of phase change.

5.3.2 MTU-LHT-1A Samples

5.3.2.1Results & Analysis

MTU-LHT-1A regolith simulant produced by the PSTDL at MTU was used in the second series of experimental tests for detecting volatile phase change. The thermal and mechanical properties of this lunar simulant have been classified in part through these experimental tests and tests conducted by other members of the PSTDL. Compaction and relative bulk density has shown to play a significant role in tests conducted with this simulant. Bulk densities for this material range from 1.2 g/cm^3 (lightly compacted) to 1.86 g/cm^3 (heavily compacted). The thermal conductivity for MTU-LHT-1A was calculated using the temperature profiles from the dry 50 W test and equation 1. The calculated thermal conductivity ranged from 0.32 to 0.42 $W/(mK)$ (Figure 30) given a thermocouple placement error of ± 1 mm, and the sample bulk density for this test was ~1.7 g/cm^3.

Results from experimental tests with 0 wt.% water, 1.5 wt.% ice, 5 wt.% water, 5 wt.% ice, 7 wt.% water, 10 wt.% water, and 10 wt.% ice can be seen in Figures 31 through 36 included in the appendix. Similar to the results of the mixed silica sand tests, inflection points denoting a change in thermal conductivity before and after phase change regions are more pronounced with an increase in volatile composition. Regions of latent heat were generally more distinguishable at the heater surface, 5 mm, and 10 mm from the surface during the constant 50 W tests. This conclusion was determined by visualizing the temperature profiles of each power level and thermocouple location across all weight percentages of water or ice (Figures 37 to 45).

Figures 46 and 47 show the temperature profiles measured by thermocouples located at the surface of the heater out to a distance of 15 mm in a 5 wt.% ice and 10 wt.% ice mixed sample with a 50-Watt power supply. These figures also show the rate change of temperature for these profiles which is useful to distinguish inflection points along the temperature curves. These inflection points in the temperature curves indicate the bounds of phase change as the thermal conductivity of the material changed and energy was absorbed by the vaporization, or melting, regions of phase change. Figure 48 shows the same rate change of temperature overlayed on the temperature profile for a silica sand

test at 100 Watts with 5 wt.% water content, but provides a clearer depiction of these inflection points, or peaks in the rate change of temperature. These peaks bounding the vaporization region were identified for all MTU-LHT-1A tests with water and ice inclusions, though phase change wasn't observed out to 10 mm for tests with higher water or ice content (Figure 50).

This method of distinguishing regions of phase change using inflection points yielded information about the periods required for the phase change to complete at known radial distances or known volumes of mixed samples at each constant power level.

The time at which phase change completed for a known volume of a mixed sample was then used to set an upper limit for integration on each respective weight percentage temperature profile from the surface of the heater out to 10 mm. In conjunction with the integration of the temperature profiles for each mixed sample, the upper limits were used to perform multiple integrations on the constant power dry sample temperature profiles.

The resulting pair of integrals from the mixed sample temperature profiles and the dry temperature profiles occur over the same period with the same amount of power supplied to the heat source. The difference between the energy content of the dry test temperature profiles and each mixed sample temperature profile represents the relative amount of energy being absorbed by the latent heat of vaporization of the water content in the mixed sample.

To estimate the water content for an unknown sample the difference between the energy content of the dry test temperature profiles and the energy content of the mixed sample temperature profiles can be divided by the original energy content of the dry temperature profiles and multiplied by an integral of the recorded constant power data using the same respective upper time period limit. This will yield an energy value represented in Joules. The latent heat of vaporization for water is known to be 2260 kJ/kg [6] which can be divided into the energy absorbed by the phase change resulting in an approximation of the mass of water. This mass of water can be divided by the difference between the small sample volume's total mass, found by multiplying the measured bulk density by the volume of a cylinder surrounding the heater out to a known radius, and the mass of water to find the approximate weight percentage of water relative to the dry mass of MTU-LHT-1A in the mixed sample.

This series of calculations were performed on the 50-Watt test data to try and approximate the known moisture content given only the dry temperature profile test data and the temperature profiles for 5 wt.%, 7 wt.%, and 10 wt.% water mixed samples. Using the volume from the surface of the heater out to the second thermocouple located 5 mm from the heater surface an estimated moisture content of 6.49 wt.% was calculated for the mixed sample containing a known moisture content of 5.81 wt.%. However, the calculation quickly diverged when attempting to approximate the weight percentage of the 7 wt.% and 10 wt.% tests, resulting in estimated values around 17.08 wt.% and 246.5 wt.% respectively.

These larger deviations in weight percentage approximation are likely a result of compounding errors and uncertainties in the data collected. The thermocouple placement error of ± 1 mm results in significant changes in the small sample volume surrounding the heater used in this energy balance estimation, with the bulk density measurement being reliant on a scale with ± 2 gram and sample column measurements within ± 0.125 inches. Other factors that could be accounted for would be heat released through the top of the heater and a better approximation of the volume of heat region surrounding the probe. Aside from the listed sources of potential error, an approximation of an unknown weight percentage of water in a mixed sample of MTU-LHT-1A was achieved and can be applied to other constant power levels and mixed samples.

Further tests in a vacuum environment will determine if the weight percentage of volatiles can be determined to be within ± 1 wt.% given the difference in thermal conductivity imposed by the environment. Thermistors with a higher sensitivity may need to be considered in addition to more experimental tests before this conclusion can be asserted.

5.4 Conclusions

These experimental tests have proven that distinguishable differences in phase change periods can be detected and measured using a constant heat source and thermistors. Testing has provided insight into the power requirements and heat flux necessary to accomplish the desired accuracy of measurement. Localized pressure within a compacted and cemented icy mixed sample has been alluded to in the results as phase change has occurred at unexpected temperature ranges. Since the identification of the volatile species is largely reliant on known temperature and pressure-dependent phase change behavior, solutions to this observed phenomenon will need to be investigated further. Additional testing under cryogenic and vacuum conditions will provide more useful data for these correlational studies. Upcoming testing with a controlled constant temperature heat source will also be investigated to determine the best method of control for detecting these crucial phase change regions. Knowledge of the relative compaction levels of the volatile infused regolith will be critical in the detection and quantification of volatiles which makes the integration of a calorimetric device and a dynamic percussive cone penetrometer appealing as this data will be collected by the same instrument and utilized by the thermal measurement subsystem.

The water content for a 50-Watt test with 5.8 wt.% water was calculated to be 6.49 wt.% which is within ± 1 wt.% indicating that it is possible with the proposed method, however further work will be required to draw better correlations between these observations. Data collected thus far has proven the method of detection is feasible and the design, manufacturing, and testing of a thermal cone for the PHCP has begun. The thermal cone will have a controllable heat source and temperature measurement sensors positioned along the sheathed exterior at known distances from the heat source.

6 Future Work

The experimental tests outlined in this report have aided in the development and design of the PHCP instrument. A thermal cone was designed and manufactured to implement the successful method of detecting water through the combination of a heater and thermocouples. The current design of the thermal cone includes a wound nichrome wire heat source and thermocouples spaced 5 mm, 10 mm, and 15 mm from the heat source located on the exterior of the cone instrument (Figure 52). The heater is thermally isolated from the geotechnical cone measurement system by a G-10 collar that contains mounting locations for the three 40-gauge K-type thermocouples.

The first design iteration of this thermal cone is currently being tested at low vacuum (7 mTorr) in mixed MTU-LHT-1A samples containing 0 wt.%, and 5 wt.% ice at -60°C. Each test bed is prepared in a stainless-steel box that is liquid nitrogen cooled on 4 sides to maintain this -60°C sample temperature. Preliminary tests have shown similar results to those detailed in this report, however, due to the low atmospheric pressure, regions of ice phase change are observed at much lower temperatures. Results from these tests will be published at a later date once the thermal cone design and testing are complete.

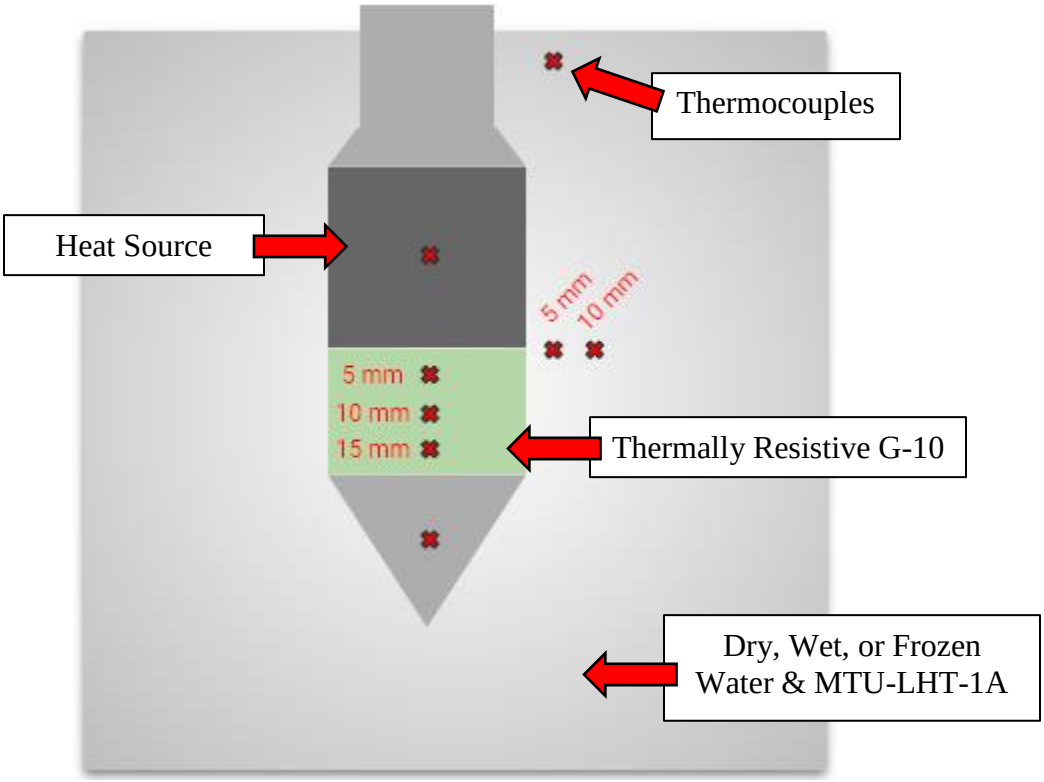

Figure 52: Simplified thermal cone design and test setup configuration

In addition to the development of the thermal cone and vacuum testing with water and ice mixed in lunar simulant, a test setup is being designed and manufactured for detecting additional volatiles such as CO_2, CH_4, C_2H_4, CH_3OH, and SO_2 which were observed by the LRO after the LCROSS impact. [1] This experimental setup will attempt to verify the same method of phase change detection and quantification of volatiles.

The design currently consists of a vacuum vessel that will be submerged in a liquid nitrogen bath to maintain sample temperatures as low as -160^{o}C (Figure 53). A custom feedthrough was manufactured to pass electrical power to a DC ceramic heater and allow small gauge thermocouples to be embedded in the surrounding lunar regolith simulant and volatile mixed sample. As heat is added to the mixed sample, regions of volatile phase changes will be observed via temperature measurements and in conjunction, a gas analysis of vaporized volatiles will be used to determine the quantity of the volatiles in the sample. This experimental setup will be validating the proposed method of volatile detection to be used by the PHCP under vacuum conditions and cryogenic temperatures similar to lunar cold traps.

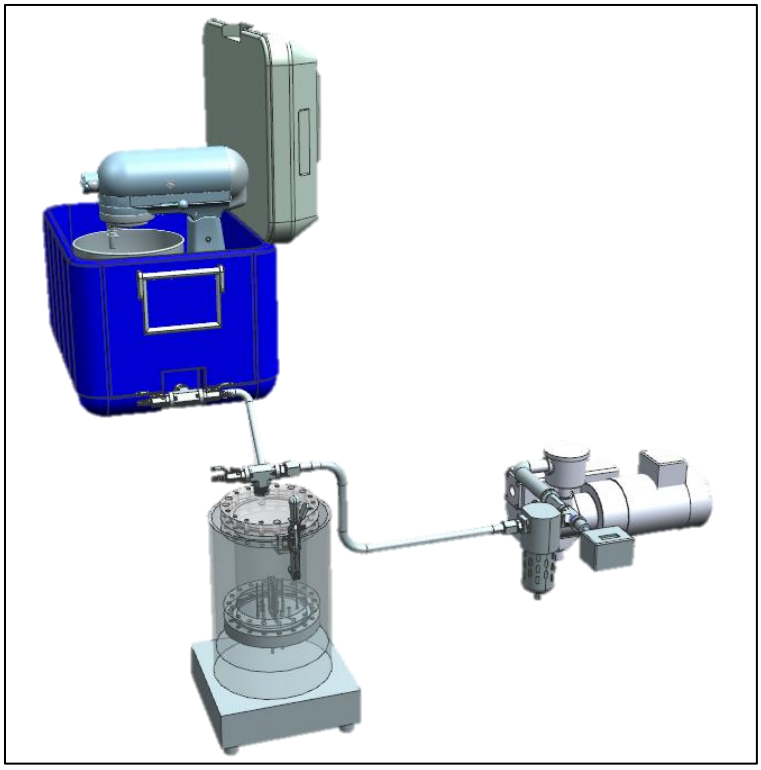

Figure 53: CAD model of the volatile experimental test setup consisting of a volatile mixing setup, LN_2 cooled vacuum vessel, and vacuum pump.

7 Reference List

[1] A. Berezhnoy, E. Kozlova, M. Sinitsyn, A. Shangaraev, and V. Shevchenko, "Origin and stability of lunar polar volatiles," *Advances in Space Research,* 2012.

[2] D. M. Hurley, D. J. Lawrence, D. B. J. Bussey, R. R. Vondrak, R. C. Elphic and G. R. Gladstone, "Two-dimensional distribution of volatiles in the lunar regolith from space weathering simulations," *Geophysical Research Letters,* vol. 39, 2012.

[3] "Sand – Density – Heat Capacity – Thermal Conductivity" material-properties.org https://material-properties.org/sand-density-heat-capacity-thermal-conductivity/ (accessed November 07, 2022)

[4] Ghafoori, Yaser & Maček, Matej & Vidmar, Andrej & Riha, Jaromir & Kryžanowski, Andrej. (2020). Analysis of Seepage in a Laboratory Scaled Model Using Passive Optical Fiber Distributed Temperature Sensor. Water. 12. 367. 10.3390/w12020367.

[5] "Heat Transfer – Conduction of Heat" enggcyclopedia.com https://www.enggcyclopedia.com/2011/09/heat-transfer-conduction-heat/ (accessed November 30, 2022)

[6] "Water – Heat of Vaporization vs. Temperature" engineeringtoolbox.com https://www.engineeringtoolbox.com/water-properties-d_1573.html (accessed November 30, 2022)

Published Works

[7] P. J. v. Susante, G. B. Johnson, S. M. Zerbel and K. A. Zacny, "Melting Ice Under Martian and other Environmental Conditions for ISRU," in ASCEND, Las Vegas, 2021.

[8] G. Johnson, A. R. P. J. v. S. Travis Wavrunek, T. Eisele and J. S. Allen, "Method for Thermal Modeling and Volatile Measurement of Lunar Regolith," in ASCE Earth & Space, Denver, 2022.

[9] M. C. Guadagno, P. J. v. Susante, G. Johnson, Z. Crook, I. Genther, T. Gronda, D. King, E. Ladensack, T. Lupinski, T. Rahkola, C. Schaefer, G. TenBrock and E. VanHorn, "Testing of Bucket Ladder Excavation Mechanism in a Dusty Thermal Vacuum Facility for Lunar Applications," in ASCE Earth & Space, Denver, 2022.

[10] B. Mellerowicz, K. Zacny, J. Palmowski, B. Bradley, L. Stolov, B. Vogel, L. Ware, B. Yen, D. Sabahi, A. Ridilla, H. Nguyen, D. Faris, P. v. Susante, G. Johnson, N. E. Putzig and M. Hecht, "RedWater: Water Mining System for Mars," Mary Ann Liebert, p. 55, 2021-2022.

8 Appendix

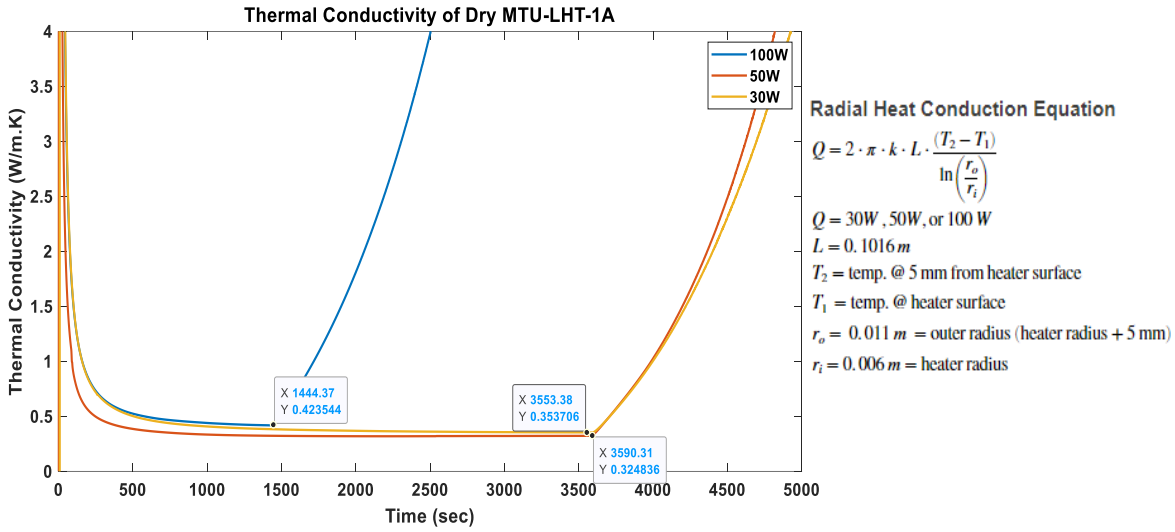

Figure 30: Thermal conductivity of MTU-LHT-1A calculated using the radial heat conduction equation on dry 100-Watt, 50 Watt, and 30-Watt tests. Ranges from 0.32 to 0.42 W/m. K

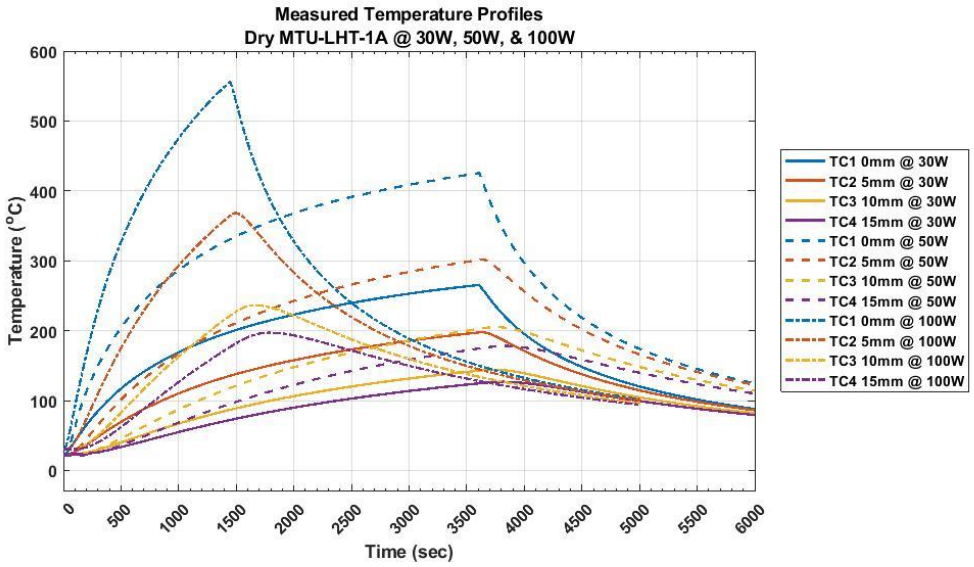

Figure 31: Temperature profiles around the cartridge heater midsection observed for constant 30-Watt, 50-Watt, and 100-Watt tests in dry MTU-LHT-1A lunar regolith samples.

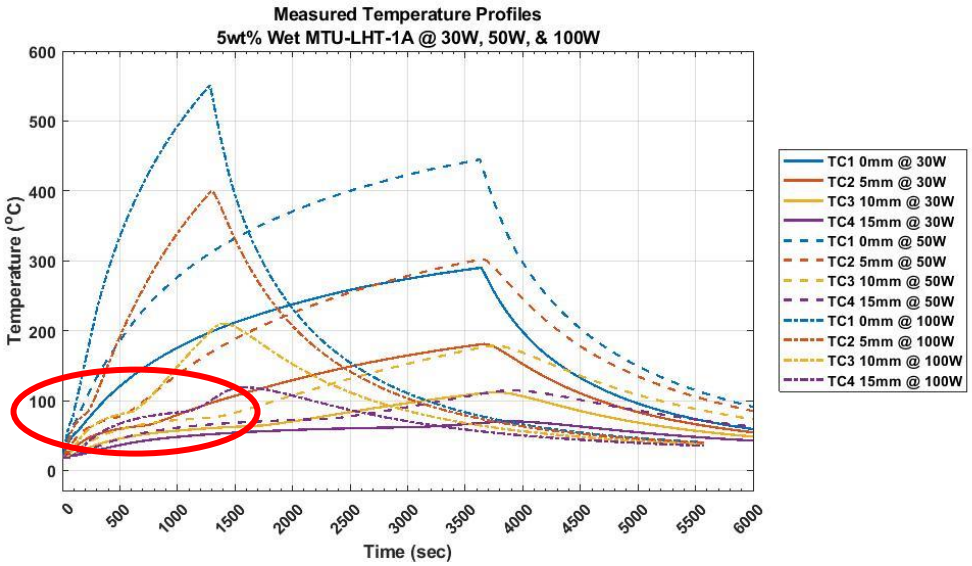

Figure 32: Temperature profiles around the cartridge heater midsection observed for constant 30-Watt, 50-Watt, and 100-Watt tests in mixed 5 wt.% water and MTU-LHT-1A lunar regolith samples.

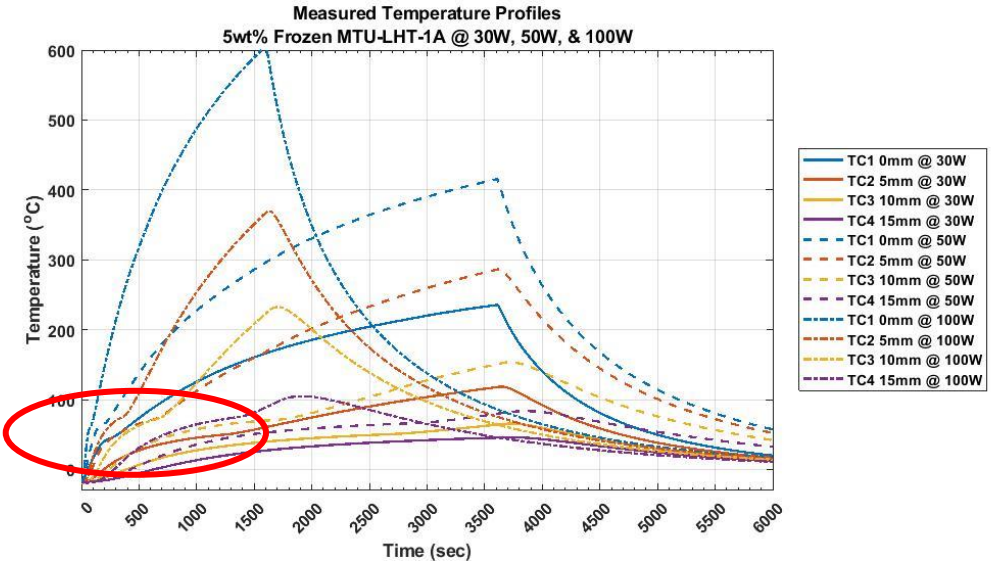

Figure 33: Temperature profiles around the cartridge heater midsection observed for constant 30-Watt, 50-Watt, and 100-Watt tests in mixed 5 wt.% concreted ice and MTU-LHT-1A lunar regolith samples.

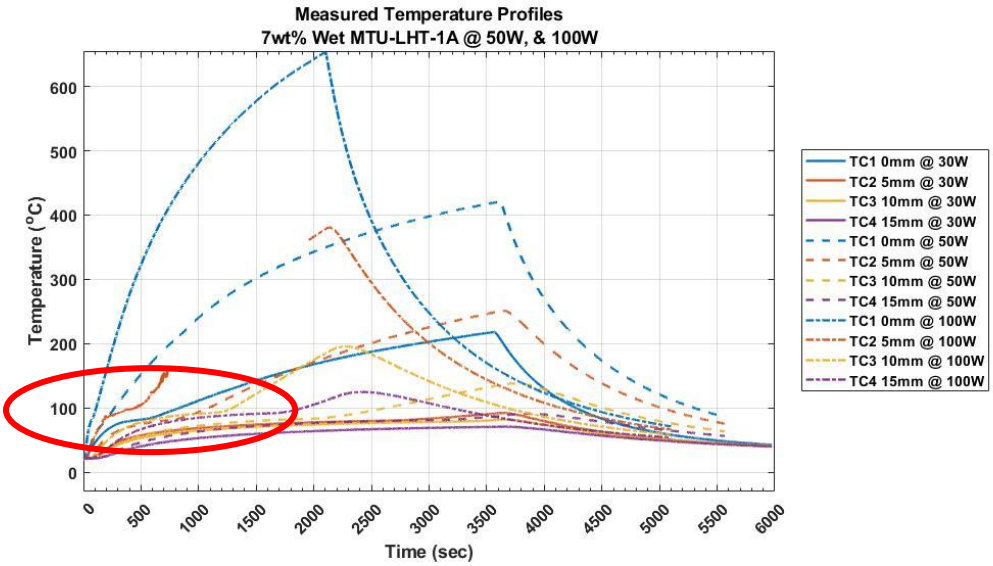

Figure 34: Temperature profiles around the cartridge heater midsection observed for constant 50W and 100W tests in mixed 7 wt.% water and MTU-LHT-1A lunar regolith samples.

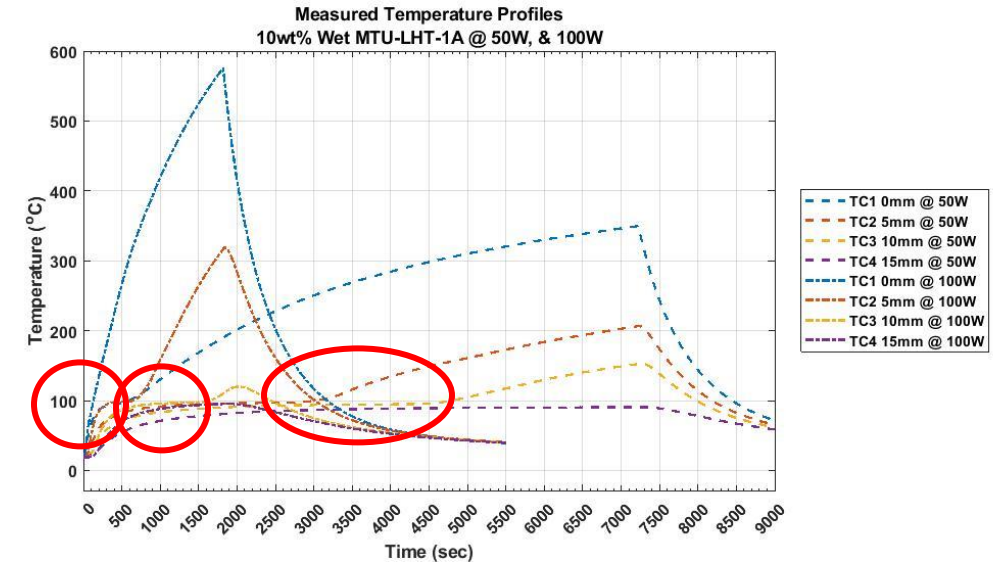

Figure 35: Temperature profiles around the cartridge heater midsection observed for constant 50W and 100W tests in mixed 10 wt.% water and MTU-LHT-1A lunar regolith samples.

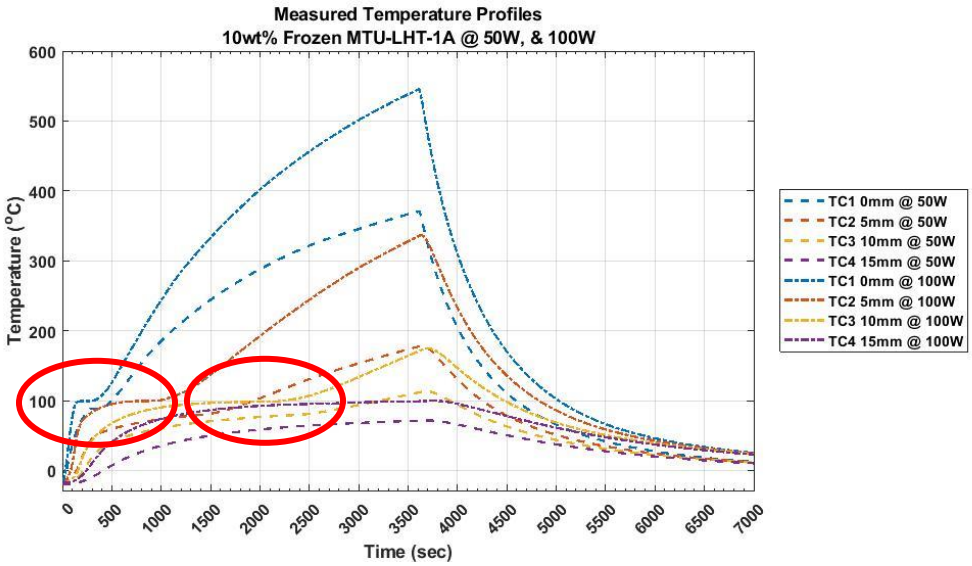

Figure 36: Temperature profiles around the cartridge heater midsection observed for constant 50W, and 100W tests in mixed 10 wt.% concreted ice and MTU-LHT-1A lunar regolith samples.

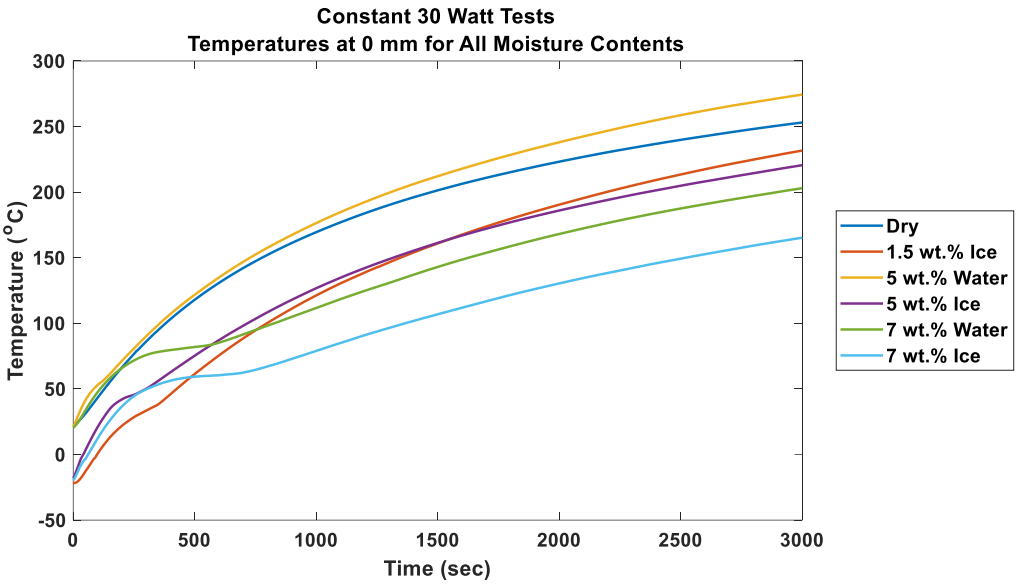

Figure 37: Temperature profiles at the surface of the heater midpoint (0 mm) for all water and ice contents tested with a constant 30-Watt power supply

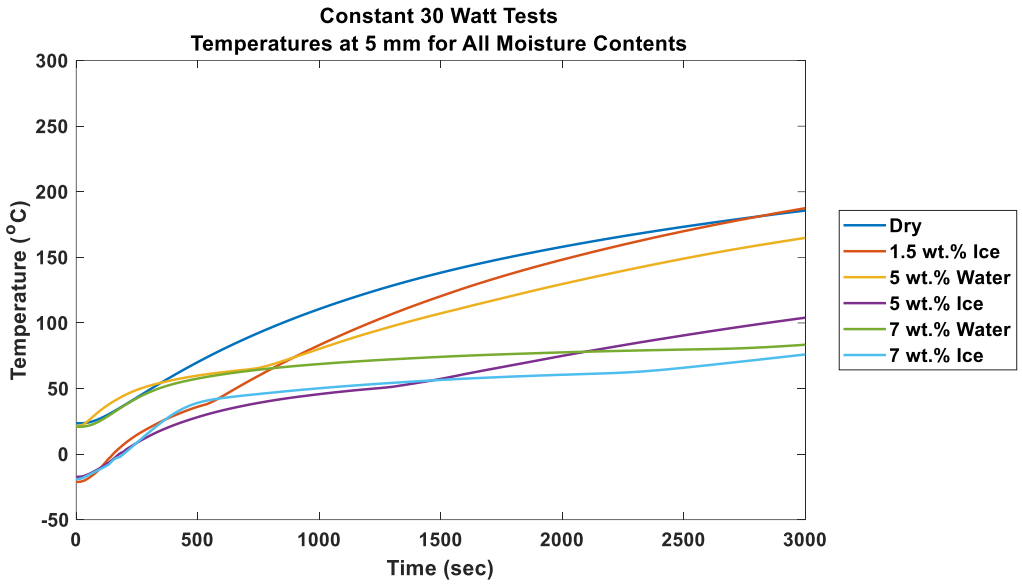

Figure 38: Temperature profiles at 5 mm from the surface of the heater midpoint (5 mm) for all water and ice contents tested with a constant 30-Watt power supply

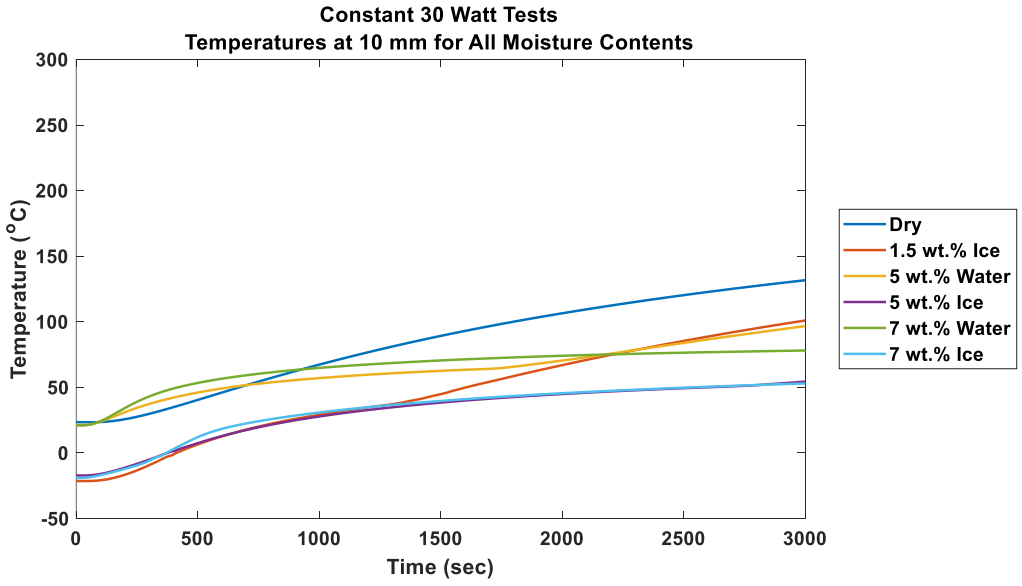

Figure 39: Temperature profiles at 10 mm from the surface of the heater midpoint (10 mm) for all water and ice contents tested with a constant 30-Watt power supply

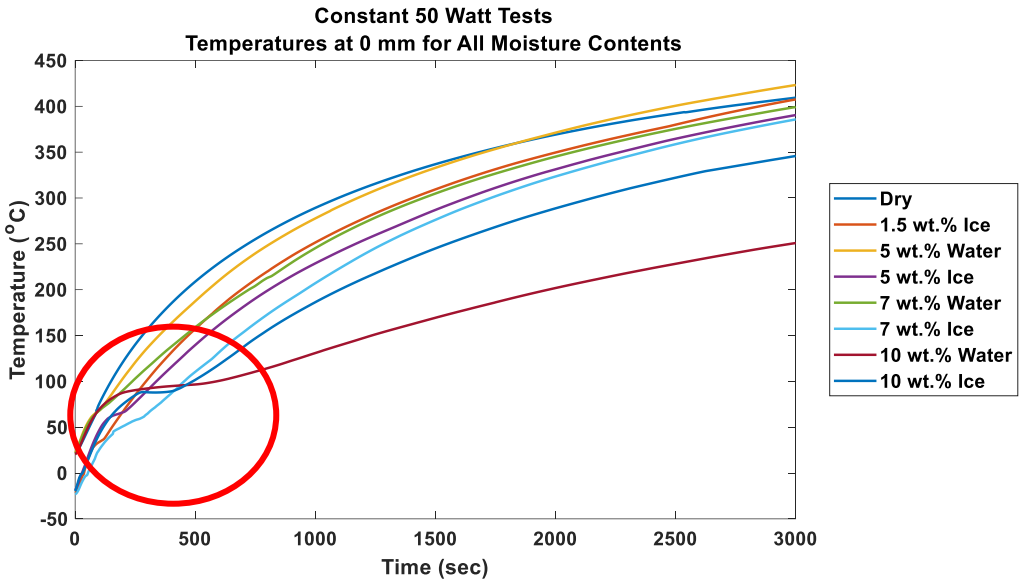

Figure 40: Temperature profiles at the surface of the heater midpoint (0 mm) for all water and ice contents tested with a constant 50-Watt power supply

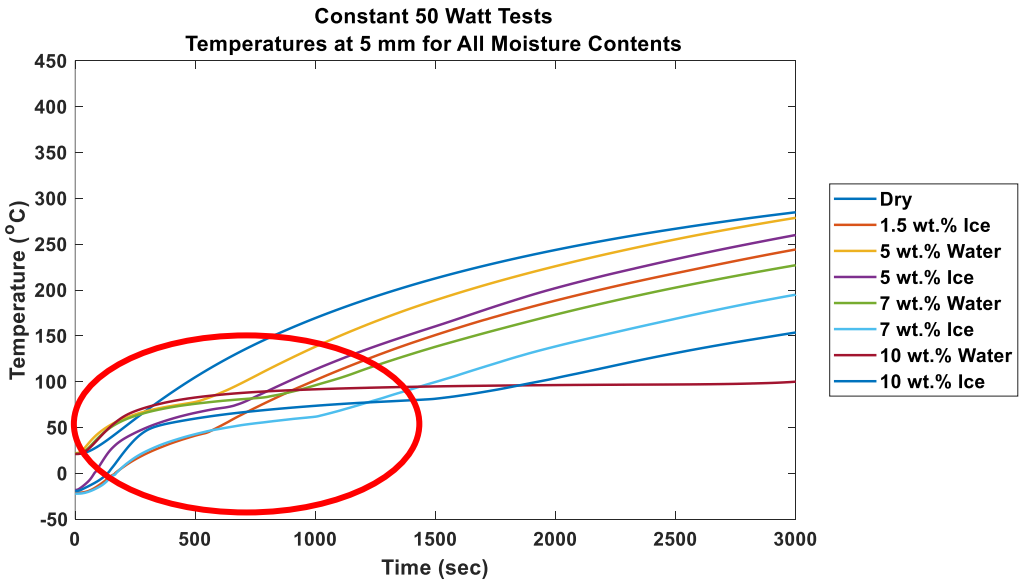

Figure 41: Temperature profiles at 5 mm from the surface of the heater midpoint (5 mm) for all water and ice contents tested with a constant 50-Watt power supply

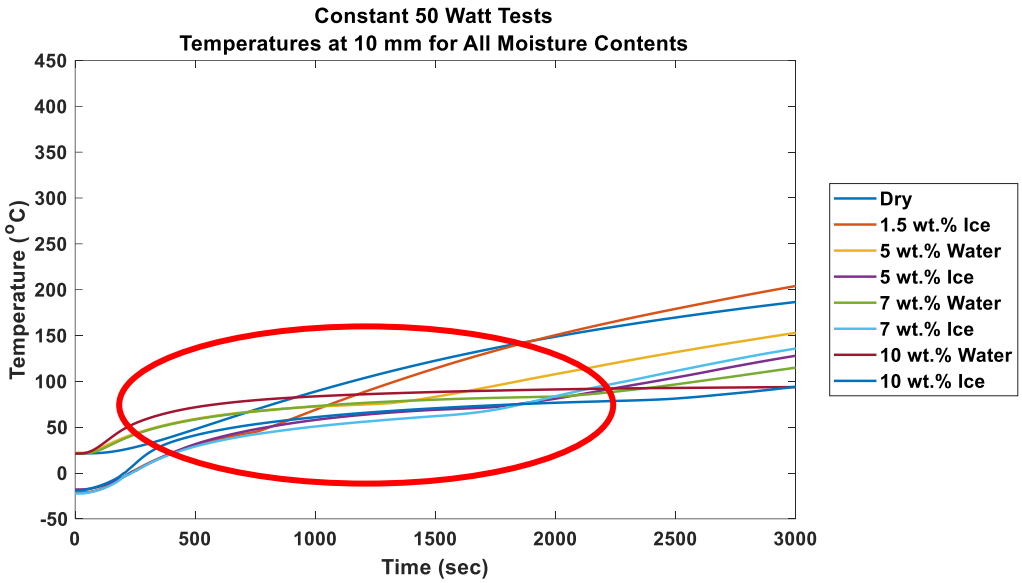

Figure 42: Temperature profiles at 10 mm from the surface of the heater midpoint for all water and ice contents tested with a constant 50-Watt power supply

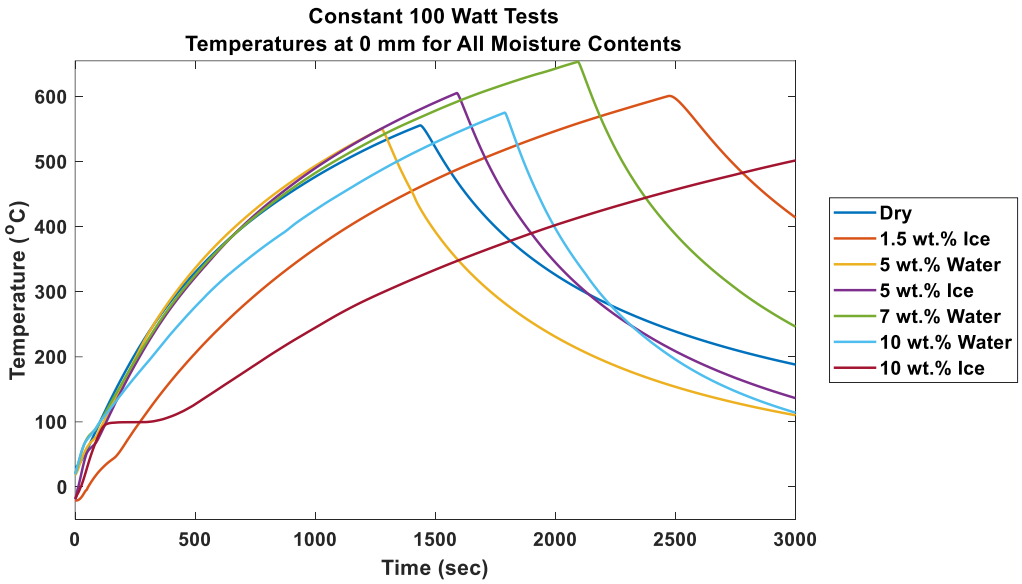

Figure 43: Temperature profiles at the surface of the heater midpoint for all water and ice contents tested with a constant 100-Watt power supply

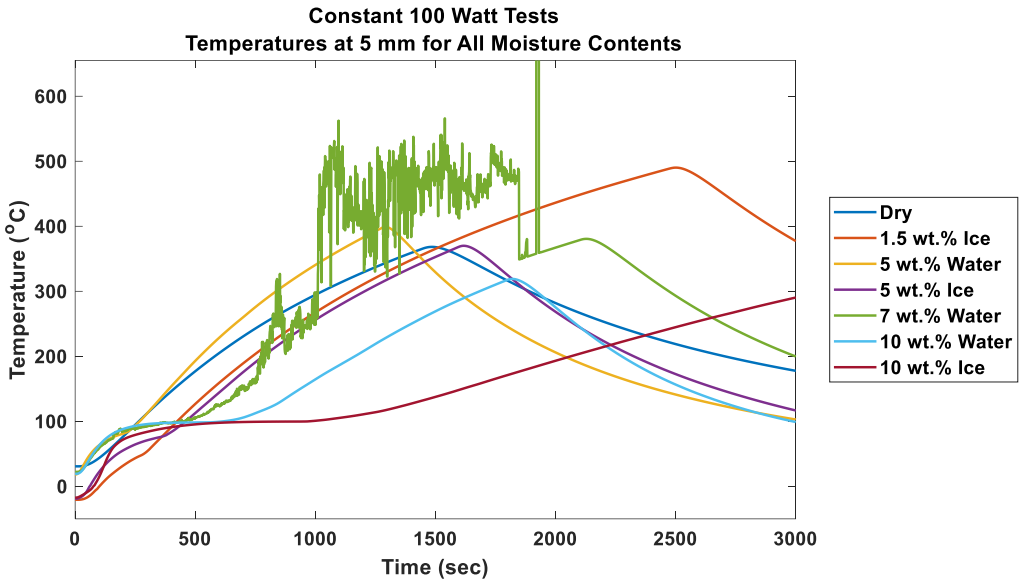

Figure 44: Temperature profiles at 5 mm from the surface of the heater midpoint for all water and ice contents tested with a constant 100-Watt power supply. 7 wt.% Water data at 5 mm included excessive noise from a loose or failing K-type thermocouple

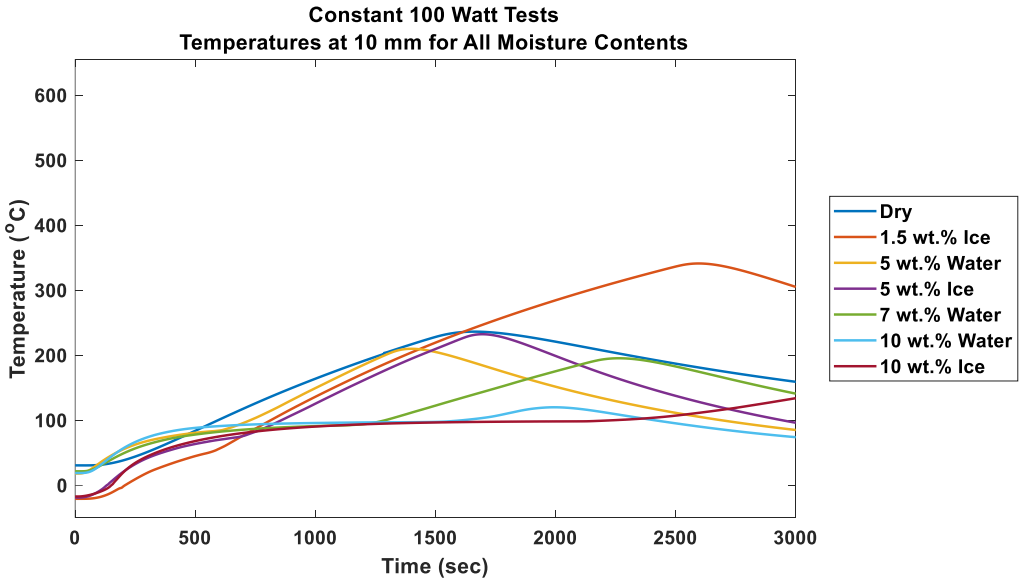

Figure 45: Temperature profiles at 10 mm from the surface of the heater midpoint (10 mm) for all water and ice contents tested with a constant 100-Watt power supply

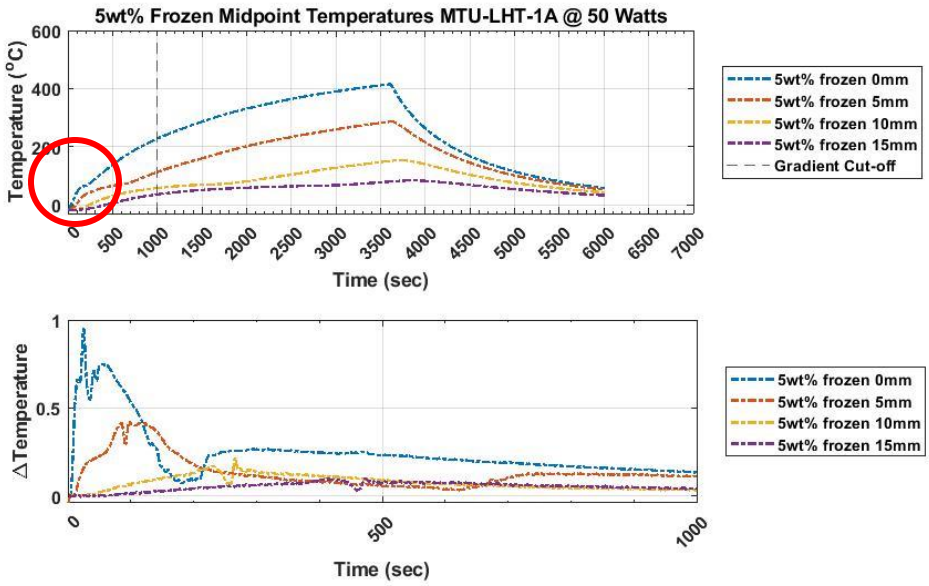

Figure 46: Temperature profiles and change in temperature over time around the cartridge heater midsection observed for constant 50W tests in mixed 5 wt.% concreted ice and MTU-LHT-1A lunar regolith samples.

9

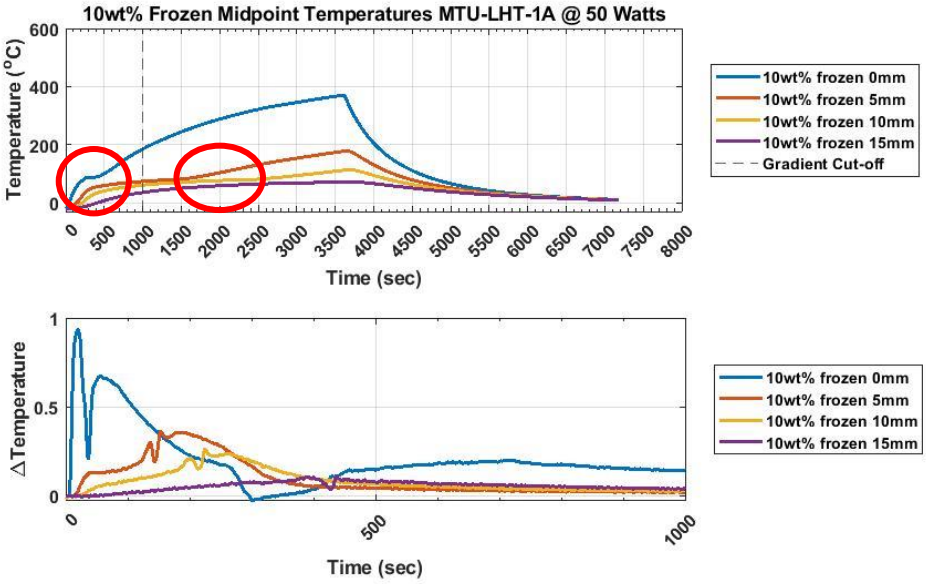

Figure 47: Temperature profiles and change in temperature over time around the cartridge heater midsection observed for constant 50W tests in mixed 10 wt.% concreted ice and MTU-LHT-1A lunar regolith samples.

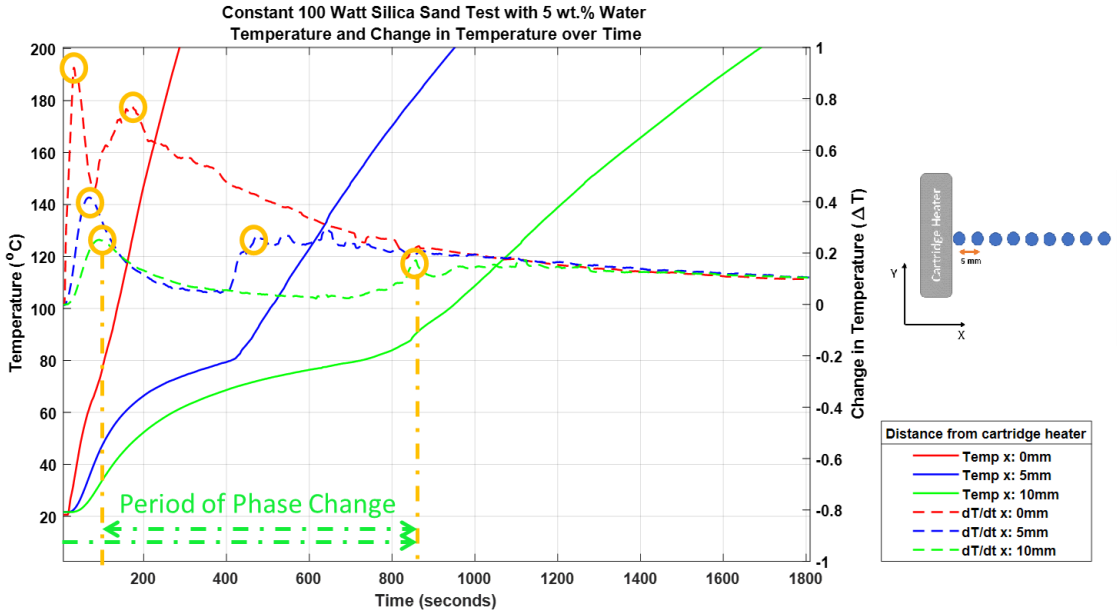

Figure 48: Temperature profiles for the first three thermocouples located at the surface of the heater, 5 mm, and 10 mm from the surface. Overlayed discrete change in temperature divided by the change in time step, showing regions of vaporization.

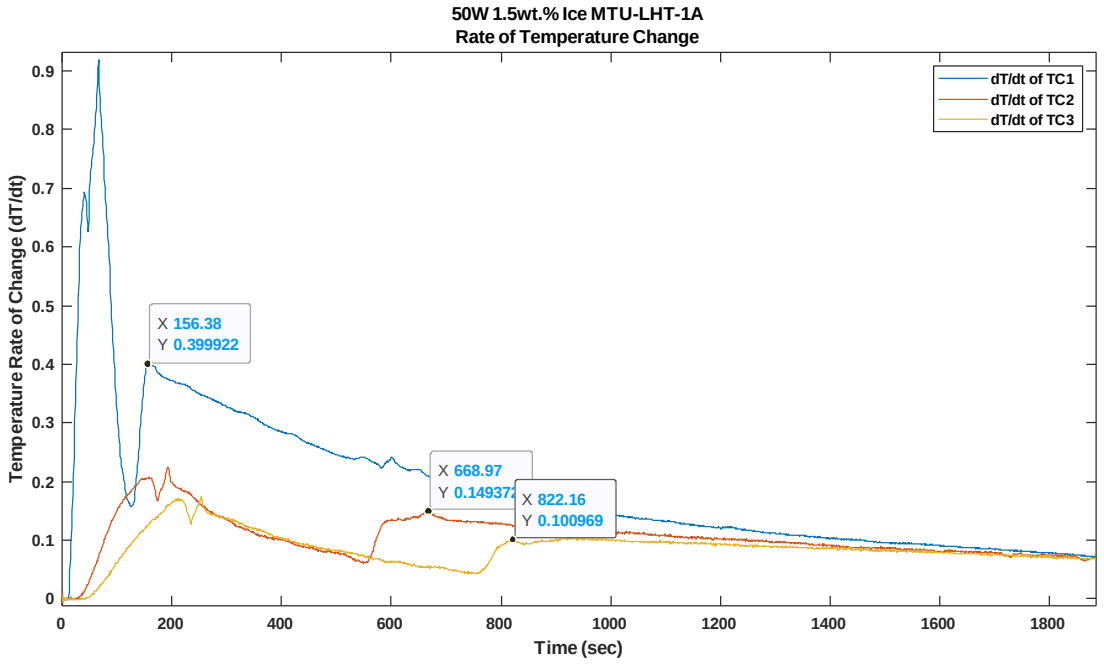

Figure 49: Rate of temperature change for the first three thermocouples located in contact with the cartridge heater surface, 5mm, and 10 mm away from the surface of the heater, TC1, TC2, and TC3 respectively. Data tips indicate the second peak rate of temperature change that indicates the end of the vaporization region.

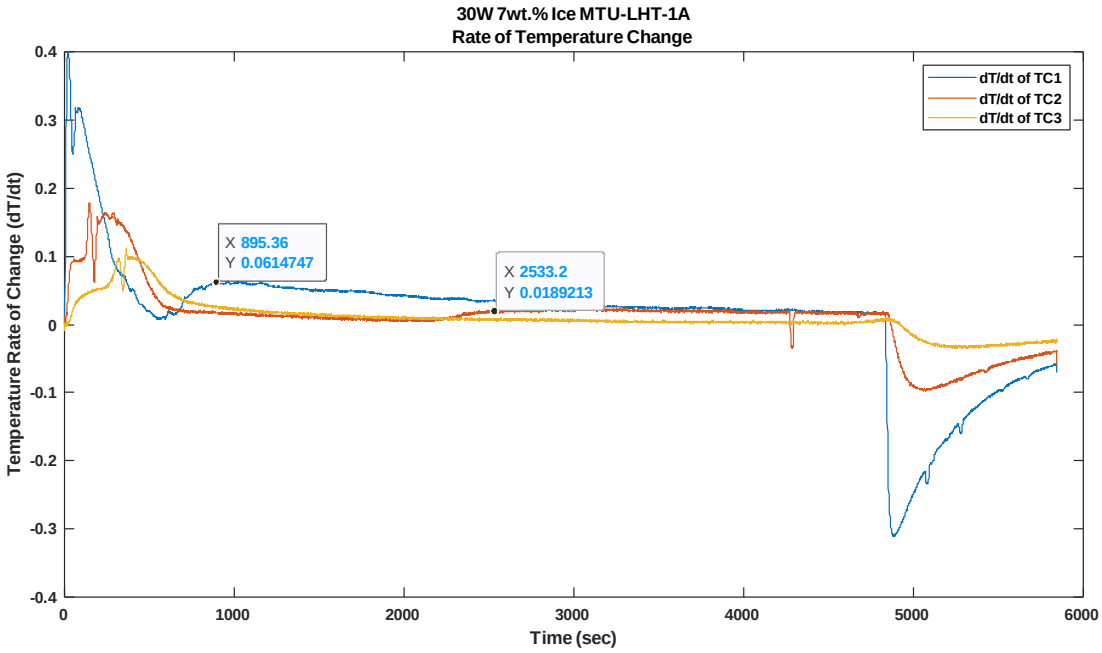

Figure 50: Rate of temperature change for the first three thermocouples located in contact with the cartridge heater surface, 5 mm, and 10 mm away from the surface, TC1, TC2, and TC3 respectively. Data tips indicate the second peak in the rate of temperature change data that indicates the end of the vaporization regions which is not observed for the 30-Watt test with 7 wt.% ice inclusion due to the high ice content and low power setting.

Figure 51: Observed dry, liquid, and frozen regions with steam evaporation during the 100-Watt test with 10 wt.% ice in MTU-LHT-1A

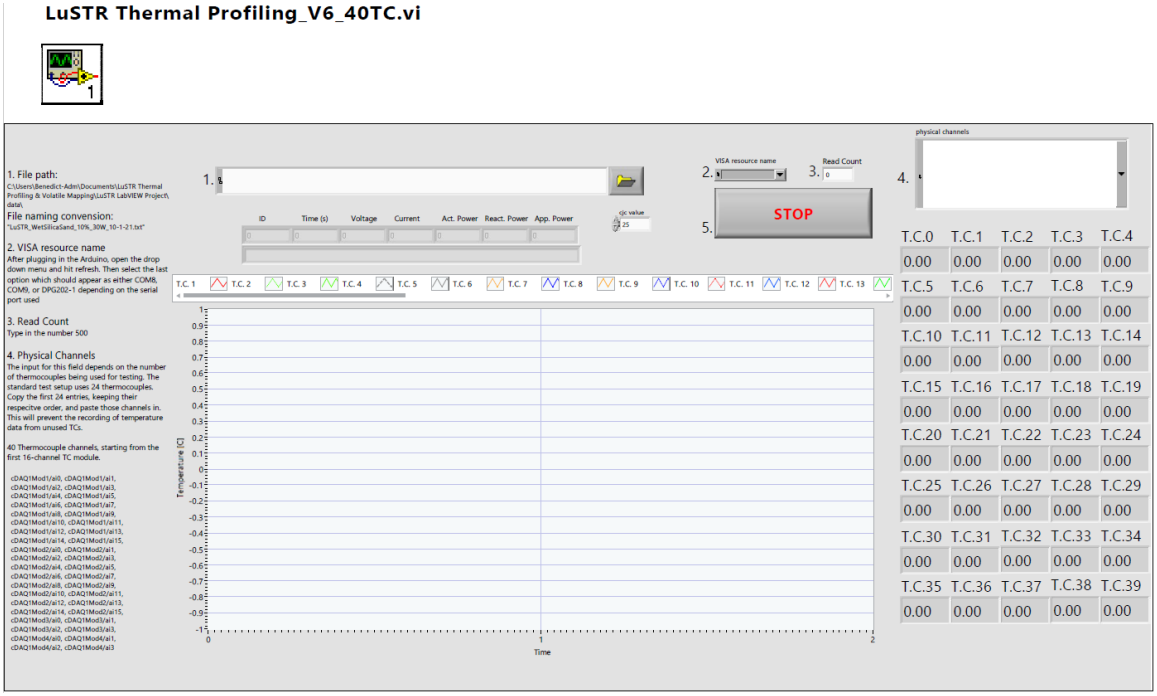

Figure 54: LABVIEW GUI, used for initializing each test, saving a .csv file, displaying temperatures, and visualizing them graphically

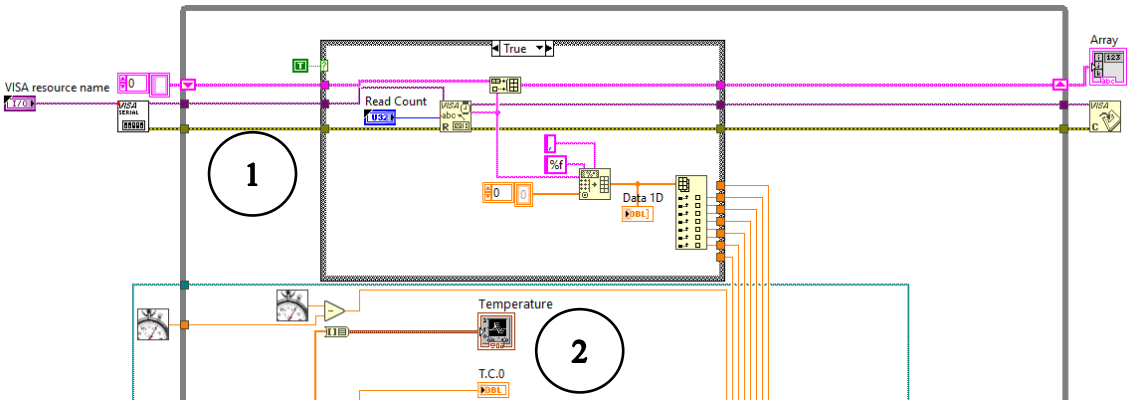

Figure 55a: LABVIEW block diagram representing part of the code responsible for (1) reading in the CSV serial data from the microcontroller monitoring voltage, current, and power supplied to the cartridge heater (2) Displaying temperature over time from up to 40 K-type thermocouples (24 used)

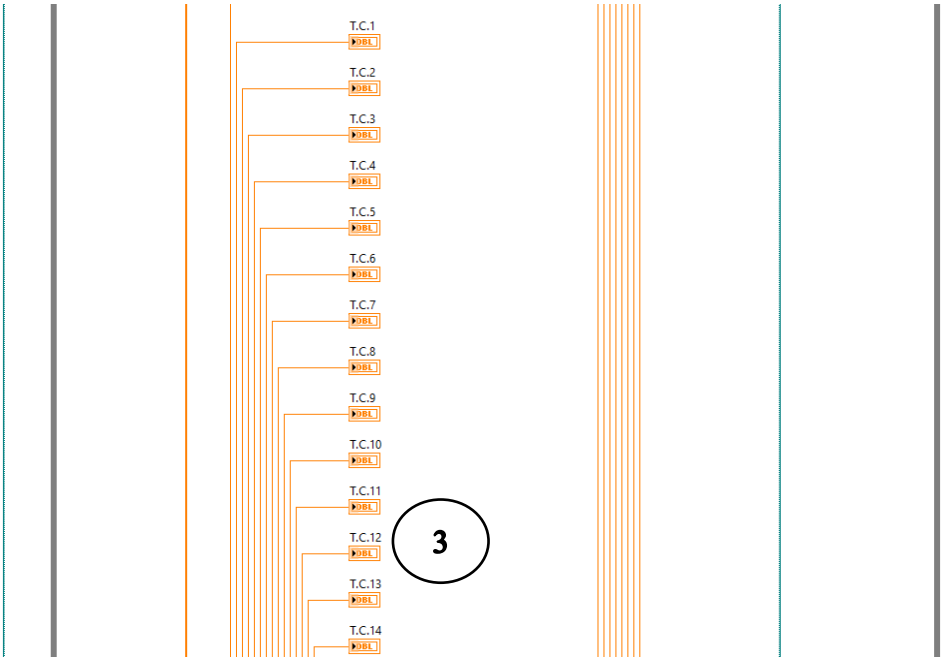

Figure 55b: LABVIEW block diagram representing part of the code responsible for displaying the numerical value of the temperatures being recorded by the K-type thermocouples (3)

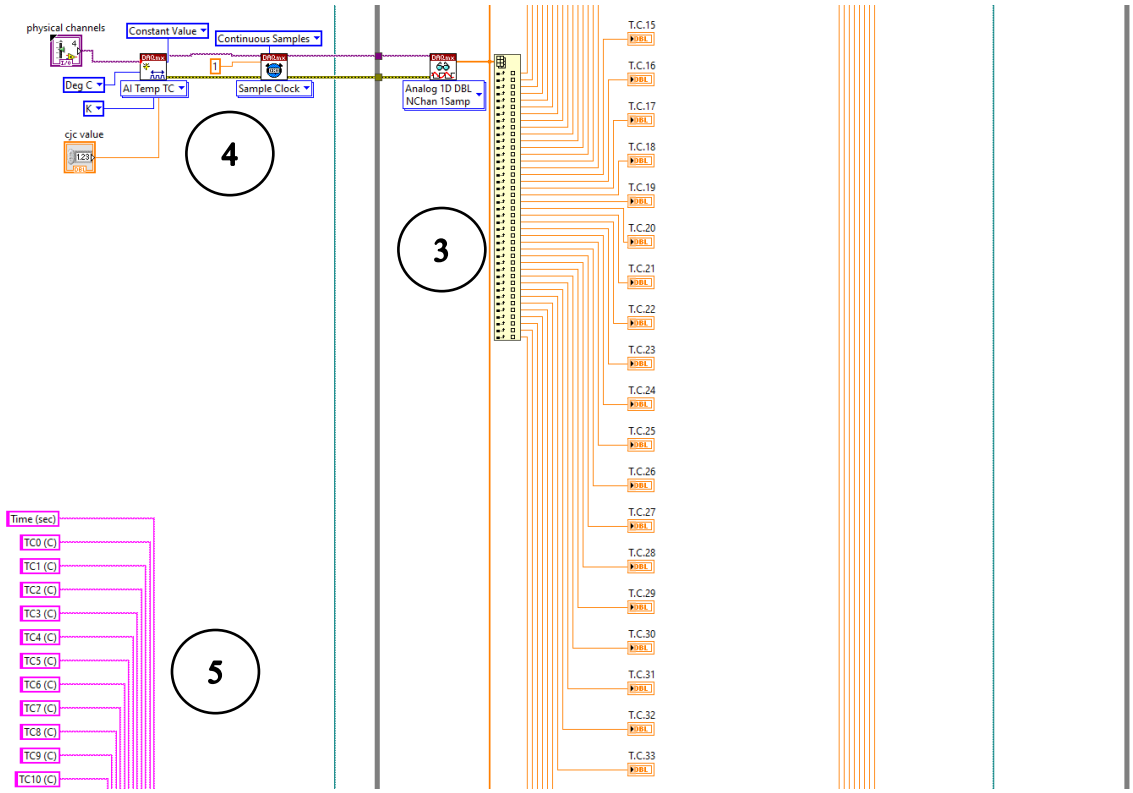

Figure 55c: LABVIEW block diagram representing the part of the code responsible for (3) displaying the numerical value of the temperatures being recorded by the K-type thermocouples, (4) reading the voltage values of the NI modules and converting the voltage to temperature while applying a cold junction compensation correction factor, and (5) applying variable column names for the final formatting of the .txt output file

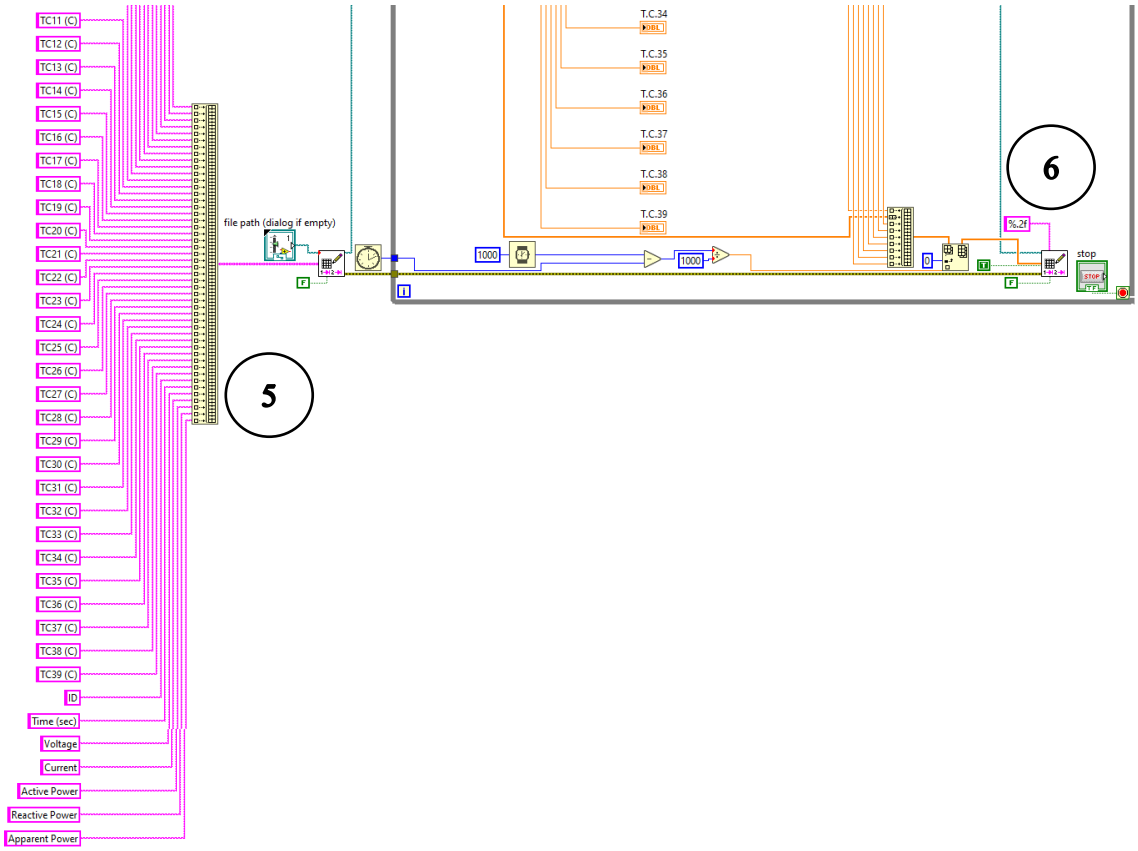

Figure 55d: LABVIEW block diagram representing the part of the code responsible for, (5) applying variable column names for the final formatting of the .txt output file, setting the file path, (6) data concatenation in the defined text file and final termination of the data acquisition code